Resonant electron transfer at metal surfaces: Theoretical analysis of scaling properties and universal behavior

U. Wille
Bereich Theoretische Physik, Hahn-Meitner-Institut Berlin, D-14091 Berlin, Germany
(Received 24 February 1994)

The resonant electron transfer processes that occur when slowly moving atoms and (positive) ions interact with metal surfaces are theoretically analyzed with regard to scaling properties and universal behavior. Within the first-order adiabatic approximation, a simple model is employed that allows a systematic (formal and numerical) study of the dependence of transition matrix elements and transition rates upon the parameters characterizing the ion-metal system. Scaling parameters are introduced, through which scale transformations of the system parameters are defined. The ion-surface distance, in particular, is scaled by means of the "classical threshold distance," below which, at given electronic energy, resonant electron transfer is classically allowed. When transformed to the scaled representation, transition matrix elements and rates are found to be expressible in terms of "reduced," universal functions, which are independent of the parameters characterizing the strength of the electronic potentials in the ion-metal system. In the limit of large ionic principal quantum numbers, the behavior of transition matrix elements and rates is largely determined by three universal functions that depend on the scaled ion-surface distance only. Scaling laws connecting transition matrix elements and rates for different ionic principal quantum numbers are established. Resonance neutralization of highly charged ions and resonance ionization of Rydberg atoms are considered as specific cases. Quasiclassical aspects and possible applications of our results as well as extensions of our analysis are briefly discussed.

I. INTRODUCTION

Resonant electron transfer is a ubiquitous process in the interaction of slowly moving atoms and ions with metal surfaces. Under the near-adiabatic conditions prevailing in this type of interaction, the one-electron potential acting in the ion-metal system[1] induces transitions in which either an atomic electron is transferred into an initially empty conduction-band state of virtually the same energy ("resonance ionization"), or a conduction-band electron is transferred into an empty ionic state ("resonance neutralization").[2,3] In specific situations, Auger-type two-electron transitions can compete with, or can occur subsequent to, the resonant one-electron transitions.

A great deal of work, both experimentally and theoretically, has been devoted to the study of resonant electron transfer processes in ion–metal-surface interactions.[2–7] In recent years, novel aspects of these processes have been revealed in extensive studies covering previously unexplored domains of the parameter space associated with the ion-metal system. Particular emphasis has been placed on the investigation of surface interactions of slow, highly charged ions,[7–10] in which multiple resonant electron transfer populates highly excited Rydberg states of the ion, thereby leading to the formation of "hollow" atoms at an early stage of the interaction. Other subjects of current interest are the destruction of laser-excited Rydberg atoms due to resonance ionization at metal surfaces,[11–14] kinematic effects on resonant electron transfer in grazing ion-surface collisions at high ion velocities (albeit low velocity component normal to the surface),[15,16] surface interactions of sputtered and desorbed atoms,[17–19] and the formation and autodetachment of negative ions at metal surfaces.[20–22]

The theoretical description of resonant electron transfer processes relies on a variety of different methods and approximations, both quantal and classical. A general framework for the quantal treatment of the electronic dynamics is furnished by the time-dependent coupled-state method,[7,23] which has been frequently applied in conjunction with model Hamiltonians of the Anderson-Newns type.[4,5,24,25] In the near-adiabatic case, an appropriate starting point for the dynamical treatment is provided by the strictly adiabatic approximation (or "fixed-ion" approximation),[7,23] in which the electronic motion in the ion-metal system is considered at fixed ion-surface distance. Within this approximation, transition rates for resonant transfer have been calculated in first-order perturbation theory (see Ref. 26, and references cited therein) as well as by means of nonperturbative methods valid at asymptotically large distances.[27,28] Full solutions of the stationary Schrödinger equation for the one-electron problem at arbitrary distances have been obtained by applying the complex-scaling method[21,29] and the coupled-angular-mode method.[20,30,31] Classical dynamics has been employed in recent analyses of multiple electron transfer in surface interactions of slow, highly charged ions.[32–34]

The present paper deals with general aspects of the theory of resonant electron transfer in the interaction of atoms and positive ions with metal surfaces. Within a quantal framework, we analyze this kind of process with regard to scaling properties and universal behavior. Scaling and universality are closely related concepts. By submitting the parameters of a physical system to appropri-

ate scale transformations, one aims at identifying universal functions that characterize the system in terms of a reduced number of parameters, and at deriving relations ("scaling laws") connecting the values of a physical quantity for different parameter values. Thereby, one hopes to be enabled to systematize and simplify the theoretical treatment. For electronic processes in the ion-metal system, the application of scaling concepts suggests itself through the large number of parameters upon which the electronic motion in this system depends. Our specific motivation for considering the scaling behavior of resonant electron transfer has arisen from qualitative similarities observed in the parameter dependence of explicitly calculated transition matrix elements and transition rates.[35]

The analysis of scaling properties and universal behavior requires the parameter dependence of resonant electron transfer to be systematically studied over a broad range. In order to achieve this goal, we resort to the first-order adiabatic approximation in conjunction with a very simple model. Most importantly, this model allows a closed-form evaluation of the relevant transition matrix elements.[26] We are therefore in a position to investigate scaling properties by formally analyzing the matrix elements and their closed-form representations as well as by examining the results of (fairly simple) numerical calculations for transition matrix elements and transition rates.

It should be pointed out at the beginning that, in a sense, the model we use may not be fully adequate for a quantitative treatment of resonant electron transfer. But even if certain details are not properly taken into account, we believe the model at least to be capable of correctly predicting qualitative trends. In particular, this holds for those of our results which involve only *relative* quantities, like ratios of transition matrix elements and rates, and which therefore will not depend crucially on model details. In any case, the scaling procedure developed here as well as our results will be useful as guidelines to future, more sophisticated work. We also note that, since particular emphasis is placed in our analysis on the limit of large ionic quantum numbers, i.e., on the quasiclassical limit, we may understand our study as an attempt to bridge the gap between the quantal treatment and the purely classical treatment of resonant electron transfer.

We have previously[35] examined scaling properties of resonant electron transfer in a specific case by solely analyzing explicitly calculated transition matrix elements and rates. A brief account of some preliminary results of the present, general analysis has been presented elsewhere.[36]

This paper is organized as follows. In Sec. II, we specify the model assumptions upon which our analysis is based. Section III deals with the definition of appropriate scale transformations for the parameters of the ion-metal system and with the representation of transition matrix elements and transition rates in terms of scaled parameters. A general, formal analysis of the scaled representations of transition matrix elements and rates is presented in Sec. IV. In Sec. V, the universal behavior of matrix elements and rates is analyzed in the limit of large ionic principal quantum numbers, and scaling laws are inferred. A summarizing discussion of our results is given in Sec. VI. Concluding remarks are made in Sec. VII, which is followed by two appendixes containing some formal details. If not stated otherwise, we use atomic units ($e=m_e=\hbar=1$).

II. MODEL ASSUMPTIONS

We consider an atom or positive ion moving slowly in front of an ideal (plane) metallic surface. Assuming the ionic motion to proceed along classical trajectories, we adopt the first-order adiabatic approximation[7,23] to describe resonant transitions between the electronic states of the ionic core, which is centered at an arbitrary, fixed distance D in front of the surface, and the states of the conduction-band of the metal (cf. the schematic diagram shown in Fig. 1). We assume the metal to be at zero temperature, so that we have to distinguish two cases:[37] (i) transitions of an electron occupying initially an ionic state with energy above the Fermi level of the metal into an empty conduction-band state, and (ii) transitions of a conduction-band electron into an empty ionic state lying energetically below the Fermi level of the metal. The latter case can be viewed as the transition of a *hole* initially bound to the ionic core into an unoccupied conduction-band *hole* state. Cases (i) and (ii) can therefore be combined by considering transitions of an electron *or* a hole (indiscriminately referred to in the following as "electron") out of an initial *ionic* state into a final *conduction-band* state.

While the strictly adiabatic approximation is the natural starting point for treating the dynamics of resonant electron transfer at low ion velocities, the range of validi-

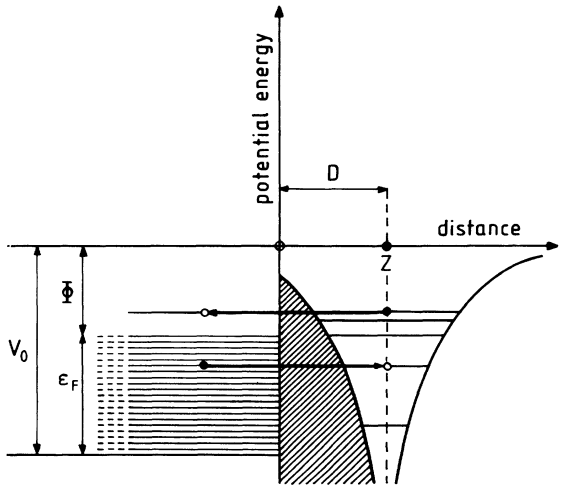

FIG. 1. Schematic diagram illustrating the shape of the electronic potential in the ion-metal system as well as the resonant electron transfer processes that can occur at the surface. D=ion-surface distance; Z=effective ion core charge; Φ=work function; ϵ_F=Fermi energy; $V_0=\Phi+\epsilon_F$=depth of conduction-band potential.

ty of the *first-order* approximation is restricted to sufficiently large distances D, where the adiabatic mixing of the ionic states caused by the metal potential is small. For the sake of completeness, we will extend our explicit calculations down to $D=0$. However, our analysis emphasizes the range of fairly large distances, particularly the vicinity of the classical threshold distance and the classically forbidden range in which resonant electron transfer can occur via quantal tunneling only.

A. Unperturbed potentials and wave functions

We use coordinates $\mathbf{r}\equiv(x,y,z)$ such that the surface coincides with the (x,y) plane and the metal fills the half-space $z\leq 0$. The ion is assumed to lie on the z axis, i.e., the coordinates of its center are $(0,0,D)$. For the electronic potential of the unperturbed ionic core V_c, we adopt the purely Coulombic form

$$V_c(\mathbf{r};D)=\frac{-Z}{|\mathbf{r}-D\hat{\mathbf{e}}_z|}\ , \tag{1}$$

where Z is the effective core charge number. Hence, the unperturbed bound states of the ionic system are represented by hydrogenic wave functions $\psi^{(Z)}_{nlm}(\mathbf{r}-D\hat{\mathbf{e}}_z)$ with spherical quantum numbers n,l,m and energy

$$\epsilon_n=-\kappa_n^2/2\ , \tag{2}$$

where

$$\kappa_n=Z/n \tag{3}$$

is the mean orbital momentum in the state with quantum numbers n,l,m (Ref. 38) (which is defined as the root of the expectation value of the momentum squared, and is identical to the classical orbital momentum).

The unperturbed conduction-band states of the metal are described within a simplified jellium model ("Sommerfeld model"),[7,39] in which the electronic potential is approximated as

$$V_m(\mathbf{r})=-V_0\Theta(-z)\ . \tag{4}$$

The potential depth V_0 is the sum of the Fermi energy ϵ_F and the work function Φ, and $\Theta(z)$ is the unit step function. The explicit form of the bound-state jellium wave functions $\phi^{(V_0)}_{\mathbf{k}}(\mathbf{r})$ corresponding to electronic momentum $\mathbf{k}\equiv(k_x,k_y,k_z)$ and energy

$$\epsilon_{\mathbf{k}}=k^2/2-V_0 \tag{5}$$

($k=|\mathbf{k}|$; the effective electron mass is taken equal to the bare mass m_e) is given in Appendix A.

For the purposes we have in mind, our choice for the unperturbed ionic and conduction-band wave functions appears to be adequate. We mention that in many typical cases (alkali atoms, highly excited Rydberg atoms, highly charged ions) one deals with effective one-electron systems, which can be accurately described in terms of hydrogenic wave functions with an adjustable effective core charge. The jellium wave functions corresponding to a step potential are sufficiently accurate if the ionic orbital considered has small amplitude only in the immediate vicinity of the surface. Simple estimates show that this condition is fulfilled already for ion-surface distances considerably smaller than the classical threshold distance.

B. Transition matrix elements

As for any rearrangement process, the transition matrix element for resonant electron transfer can be written in two equivalent forms.[40] Let us assume the total electronic potential in the ion-metal system at arbitrary distance D to have the form[41]

$$V=V_m+V_c^{>}+V_i\equiv V_m+(V_c-V_c^{<})+V_i\ , \tag{6}$$

where $V_c^{>}=V_c\Theta(z)$ and $V_c^{<}=V_c\Theta(-z)\equiv V_c-V_c^{>}$. The restriction of the ionic Coulomb potential to the "vacuum" half-space $z>0$ reflects the assumption that the ionic potential is completely screened inside the metal. The term V_i represents the sum of the classical image potentials induced by the ionic core and by the electron under consideration. We can now write the transition matrix element either in the "prior" form involving the initial-channel perturbation $V-V_c$,

$$\begin{aligned}\mathcal{M}^{\text{prior}}&=\langle\phi^{(V_0)}_{\mathbf{k}}|V-V_c|\psi^{(Z)}_{nlm}(D)\rangle\\&\equiv\langle\phi^{(V_0)}_{\mathbf{k}}|V_m-V_c^{<}+V_i|\psi^{(Z)}_{nlm}(D)\rangle\ ,\end{aligned} \tag{7}$$

or in the "post" form involving the final-channel perturbation $V-V_m$,

$$\begin{aligned}\mathcal{M}^{\text{post}}&=\langle\phi^{(V_0)}_{\mathbf{k}}|V-V_m|\psi^{(Z)}_{nlm}(D)\rangle\\&\equiv\langle\phi^{(V_0)}_{\mathbf{k}}|V_c^{>}+V_i|\psi^{(Z)}_{nlm}(D)\rangle\ .\end{aligned} \tag{8}$$

The matrix elements (7) and (8) are identical, provided the resonance condition

$$\epsilon_{\mathbf{k}}=\epsilon_n \tag{9}$$

or, equivalently,

$$k=k_n\equiv(2V_0-\kappa_n^2)^{1/2} \tag{10}$$

is fulfilled.

A simple evaluation of the matrix elements (7) and (8) is inhibited by the presence of the image-potential term V_i. In the context of the present study, we therefore have to disregard this term completely. This clearly constitutes a severe approximation, whose consequences are difficult to assess.

Without V_i in the perturbing potential, the matrix elements (7) and (8) can be evaluated in closed form for arbitrary parameter values of the ion-metal system, including the nonresonant case.[26,42] As the post form is slightly easier to handle in the actual evaluation and much better amenable to a formal discussion than the prior form, we adopt as our final expression for the transition matrix element the form (8) with V_i omitted:

$$\begin{aligned}\mathcal{M}^{(Z;V_0)}_{nlm}(\mathbf{k};D)&=\langle\phi^{(V_0)}_{\mathbf{k}}|V_c^{>}(D)|\psi^{(Z)}_{nlm}(D)\rangle\\&\equiv\int d^3r[\phi^{(V_0)}_{\mathbf{k}}(\mathbf{r})]^{*}V_c^{>}(\mathbf{r};D)\\&\quad\times\psi^{(Z)}_{nlm}(\mathbf{r}-D\hat{\mathbf{e}}_z)\ .\end{aligned} \tag{11}$$

Below, we will explicitly consider the effect that comes about by the nonorthogonality of the initial and final states in the matrix element (11). We note that in the analysis of Ref. 41, which includes a discussion of image-potential and nonorthogonality effects, the specific form (11) of the transition matrix element has been identified as a "permissible" form for use in a first-order treatment of resonant electron transfer.

An immediate simplification of the matrix element (11) arises from the presence of the potential $V_c^>$, which effectively restricts the $\mathbf{r}$ integration to the range $z \geq 0$. In the resonant case (from now on, this is the only case we consider), the wave function $\phi_{\mathbf{k}}^{(V_0)}(\mathbf{r})$ factorizes in this range (cf. Appendix A) into the penetration coefficient b, which depends on both V_0 and Z, and a "reduced" wave function $\chi_{\mathbf{k}_\parallel}^{(\kappa_n)}(\mathbf{r})$, in which the V_0 dependence has been eliminated in favor of a dependence on κ_n (and hence on Z) and which depends on the momentum vector $\mathbf{k}$ only via its component $\mathbf{k}_\parallel$ parallel to the surface. Consequently, the matrix element $\mathcal{M}_{nlm}^{(Z;V_0)}(\mathbf{k};D)$ can be written in terms of a V_0-independent, reduced matrix element

$$M_{nlm}^{(Z)}(\mathbf{k}_\parallel;D)=\langle \chi_{\mathbf{k}_\parallel}^{(\kappa_n)}|V_c^>(D)|\psi_{nlm}^{(Z)}(D)\rangle \tag{12}$$

as

$$\mathcal{M}_{nlm}^{(Z;V_0)}(\mathbf{k};D)\equiv\mathcal{M}_{nlm}^{(Z;V_0)}(\mathbf{k}_\parallel;D)=b^*M_{nlm}^{(Z)}(\mathbf{k}_\parallel;D)\ . \tag{13}$$

It is noted that we have defined in Ref. 36, for the specific case $l=0$, $\mathbf{k}_\parallel=0$, a different type of reduced matrix element, which must not be confused with the reduced matrix element introduced here.

C. Effect of nonorthogonality

At finite distances D, the initial-state wave function $\psi_{nlm}^{(Z)}(\mathbf{r}-D\hat{\mathbf{e}}_z)$ and the final-state wave function $\phi_{\mathbf{k}}^{(V_0)}(\mathbf{r})$ in the transition matrix element (11) are not orthogonal to each other, i.e.,

$$\langle \phi_{\mathbf{k}}^{(V_0)}|\psi_{nlm}^{(Z)}(D)\rangle\neq 0\ . \tag{14}$$

The ambiguity in $\mathcal{M}$ that arises from additive constant terms in the perturbing potential[41,43] can be removed by explicitly orthogonalizing the final state with respect to the initial state (or vice versa). Defining the corrected final state as [44]

$$|\hat{\phi}_{\mathbf{k}}^{(V_0)}(D)\rangle=|\phi_{\mathbf{k}}^{(V_0)}\rangle-\langle\psi_{nlm}^{(Z)}(D)|\phi_{\mathbf{k}}^{(V_0)}\rangle|\psi_{nlm}^{(Z)}(D)\rangle\ , \tag{15}$$

we have

$$\langle\hat{\phi}_{\mathbf{k}}^{(V_0)}(D)|\psi_{nlm}^{(Z)}(D)\rangle=0\ . \tag{16}$$

The matrix element describing transitions between the states $|\psi_{nlm}^{(Z)}(D)\rangle$ and $|\hat{\phi}_{\mathbf{k}}^{(V_0)}(D)\rangle$ reads

$$\begin{aligned}\hat{\mathcal{M}}_{nlm}^{(Z;V_0)}(\mathbf{k};D)&=\langle\hat{\phi}_{\mathbf{k}}^{(V_0)}(D)|V_c^>(D)|\psi_{nlm}^{(Z)}(D)\rangle\\&\equiv\mathcal{M}_{nlm}^{(Z;V_0)}(\mathbf{k};D)-\bar{V}_c^>(D)\langle\phi_{\mathbf{k}}^{(V_0)}|\psi_{nlm}^{(Z)}(D)\rangle\ ,\end{aligned} \tag{17}$$

where

$$\bar{V}_c^>(D)=\langle\psi_{nlm}^{(Z)}(D)|V_c^>(D)|\psi_{nlm}^{(Z)}(D)\rangle \tag{18}$$

is the expectation value of $V_c^>$ in the ionic state $|\psi_{nlm}^{(Z)}(D)\rangle$. While the overlap matrix element $\langle\phi_{\mathbf{k}}^{(V_0)}|\psi_{nlm}^{(Z)}(D)\rangle$ can be evaluated in closed form,[26] this is unfortunately not possible for $\bar{V}_c^>$ (Ref. 45).

In order to get a rough estimate of the effect of orthogonalization, we consider a modified transition matrix element $\check{\mathcal{M}}$ which is obtained from $\hat{\mathcal{M}}$ by replacing the potential $V_c^>$ with the full ionic Coulomb potential V_c. The expectation value of the latter potential is $\bar{V}_c=-\kappa_n^2$ [cf. Eq. (3)], and the matrix element

$$\begin{aligned}\check{\mathcal{M}}_{nlm}^{(Z;V_0)}(\mathbf{k};D)&=\langle\hat{\phi}_{\mathbf{k}}^{(V_0)}(D)|V_c(D)|\psi_{nlm}^{(Z)}(D)\rangle\\&\equiv\langle\phi_{\mathbf{k}}^{(V_0)}|V_c(D)|\psi_{nlm}^{(Z)}(D)\rangle\\&\quad+\kappa_n^2\langle\phi_{\mathbf{k}}^{(V_0)}|\psi_{nlm}^{(Z)}(D)\rangle\end{aligned} \tag{19}$$

can be evaluated in closed form.[26]

In Fig. 2, the D dependence of a typical squared matrix element $|\check{\mathcal{M}}_n^{(Z;V_0)}|^2$ (Ref. 46) calculated from Eq. (19) is shown in comparison with the matrix element obtained by omitting the overlap term proportional to κ_n^2, i.e., by disregarding orthogonalization. It is seen that the effect of orthogonalization is to smooth out the oscillations observed in the classically allowed range, which are caused by the nodes in the ionic wave function.[26] The smoothing tends to preserve fairly well the average value of the matrix element in this range. The correction effected by orthogonalization appears to be particularly small in the vicinity of the classical threshold distance $D\approx 25$ a.u. [cf. Eq. (29) below for a quantitative definition of the classical threshold distance]. In the classically forbidden range, the matrix element in which the overlap term is omitted approaches zero much faster than does the full matrix

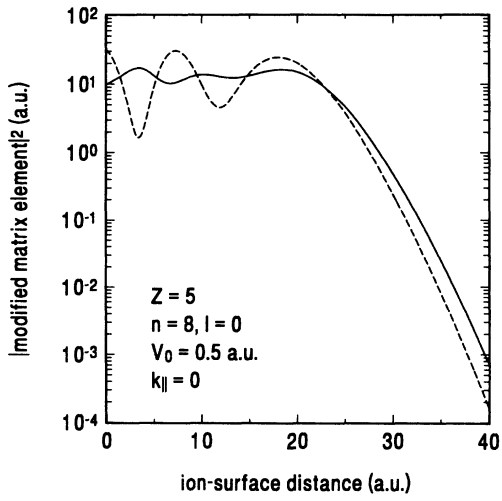

FIG. 2. Square modulus of the modified transition matrix element $\check{\mathcal{M}}_n^{(Z;V_0)}$ for the indicated parameter values, plotted as a function of the ion-surface distance D. The solid curve corresponds to the full matrix element and the dashed curve to the matrix element in which the overlap term is omitted.

element (19). This feature can be understood from a comparison of the asymptotic (large-D) behavior of Coulomb and overlap matrix elements.[26]

We assume the trends exhibited by Fig. 2 to give a qualitatively correct picture also for the effect which orthogonalization has in the original matrix element (17). For our purposes, the main conclusion then is that in a fairly broad D range centered about the classical threshold distance, orthogonalization of the final state with respect to the initial state does not change the order of magnitude of the transition matrix elements. In the following, we neglect orthogonalization and use the form (11) of the transition matrix element throughout.

D. Transition rates

Within the adiabatic approximation, the electronic transition rates at arbitrary, fixed ion-surface distance D are the quantities of primary importance. They determine, in conjunction with a prescribed time dependence of D, the time dependence of the occupation probabilities of the ionic states.[7,23,25]

In first-order adiabatic approximation, the rate for resonant transitions of an electron out to the initial state $|\psi_{nlm}^{(Z)}(D)\rangle$ into the manifold of final states $|\phi_{\mathbf{k}}^{(V_0)}\rangle$ with density $\rho(\mathbf{k})$ [or, equivalently, the decay width of the state $|\psi_{nlm}^{(Z)}(D)\rangle$] is given[7] by

$$\Gamma_{nlm}^{(Z;V_0)}(D)=2\pi\int d^3k\,\rho(\mathbf{k})\delta(\epsilon_{\mathbf{k}}-\epsilon_n)|\mathcal{M}_{nlm}^{(Z;V_0)}(\mathbf{k};D)|^2 . \tag{20}$$

For the sake of simplicity, we assume $\rho(\mathbf{k})$ to be given by the free-electron density of states, $\rho(\mathbf{k})=1/(2\pi)^3$ (for fixed projection of the electron spin). We return in Sec. VI C to a discussion of the influence which the choice of the density of states may have on our results. Now, by exploiting the invariance of $|\mathcal{M}_{nlm}^{(Z;V_0)}(\mathbf{k};D)|$ under rotations about the z axis in $\mathbf{k}$ space (in the following, the dependence of $\mathcal{M}$ on the azimuthal angle about the k_z axis via an overall phase factor[26] will be suppressed), we obtain

$$\Gamma_{nlm}^{(Z;V_0)}(D)=\frac{1}{\pi}\int_0^{k_n}dk_{\parallel}\frac{k_{\parallel}}{(k_n^2-k_{\parallel}^2)^{1/2}}|\mathcal{M}_{nlm}^{(Z;V_0)}(k_{\parallel},k_z=[k_n^2-k_{\parallel}^2]^{1/2};D)|^2 , \tag{21}$$

where

$$k_{\parallel}=|\mathbf{k}_{\parallel}|\equiv(k_x^2+k_y^2)^{1/2} . \tag{22}$$

The integration limit k_n, which has been defined in Eq. (10), can be viewed as the radius of the spherical "resonance surface" in the momentum space of the metal electrons.[15] Now, by using Eqs. (13) and (A7), we can rewrite the transition rate in terms of the reduced transition matrix element $M_{nlm}^{(Z)}(k_{\parallel};D)$ as

$$\Gamma_{nlm}^{(Z;V_0)}(D)=\frac{2}{\pi V_0}\int_0^{k_n}dk_{\parallel}k_{\parallel}(k_n^2-k_{\parallel}^2)^{1/2}|M_{nlm}^{(Z)}(k_{\parallel};D)|^2 . \tag{23}$$

As the singular term in the first factor of the integrand in Eq. (21) has been compensated by the factor $|b|^2$, the $k_{\parallel}$ integration in Eq. (23) is easily performed numerically.

We note that it is important to have $k_{\parallel}$ as the integration variable in Eqs. (21) and (23). Had we chosen k_z instead, we would have not been able to introduce a reduced transition matrix element that is independent of V_0.

Upon reversal of the sign of the magnetic quantum number m, the matrix element $\mathcal{M}_{nlm}^{(Z;V_0)}$ is merely multiplied by a phase factor.[26] Hence, the transition rate $\Gamma_{nlm}^{(Z;V_0)}$ does not depend on the sign of m, and we can confine ourselves in the following to considering the case $m\geq 0$.

III. SCALING PARAMETERS

Having specified the model assumptions that underlie our analysis, we now develop a scaling procedure for the parameters characterizing the ion-metal system. We select appropriate scaling parameters, which serve to perform scale transformations of the system parameters. Scaled representations of the transition matrix elements and transition rates are obtained by expressing these quantities in terms of the scaled system parameters.

A remark is in order here concerning the quest for "appropriate" scaling parameters. Clearly no systematic strategy exists by which an optimized set of scaling parameters can be found, i.e., a set of parameters which allows an optimal systematization and simplification of the theoretical treatment. We therefore have to resort essentially to "guessing" parameters, taking as a guideline simple physical arguments and the evidence we have obtained from calculations done previously for specific cases. Whether or not this procedure leads to the desired goal can be assessed only *a posteriori*.

Considering now the transition matrix elements, we can confine ourselves, in view of the form (23) of the transition rate, essentially to the discussion of the reduced matrix elements $M_{nlm}^{(Z)}(k_{\parallel};D)$. These matrix elements depend on the (independent) continuous parameters Z, $k_{\parallel}$, and D. As the effective charge number Z is dimensionless, we do not submit it to a scale transformation. The scale transformations defining the *scaled* parameters $\tilde{k}_{\parallel}$ and $\tilde{D}$ associated with the parallel momentum $k_{\parallel}$ and the ion-surface distance D, respectively, are introduced as

$$\tilde{k}_{\parallel}=k_{\parallel}/k_s \tag{24}$$

and

$$\tilde{D}=D/D_s , \tag{25}$$

with *scaling* parameters k_s and D_s. We require the scaled parameters to be *dimensionless,* so that k_s and D_s are required to have dimension of a momentum and a length, respectively.

The specific form of k_s and D_s is determined by looking for parameters characterizing the momentum and length scales in the ion-metal system. Characteristic quantities setting the momentum scale in the initial ionic state and in the final conduction-band state, respectively, are the orbital momentum κ_n [cf. Eq. (3)] and the magnitude of the resonant jellium-electron momentum, k_n [cf. Eq. (10)]. By choosing k_n as a scaling parameter, we would reintroduce a V_0 dependence into the analysis. We therefore define

$$k_s=\kappa_n\equiv Z/n \ . \tag{26}$$

As no characteristic length can be associated with the conduction-band states, we have to define D_s in terms of quantities related to the initial ionic state and/or to the perturbing potential. A simple choice is the classical orbital radius r_n of the manifold of states with principal quantum number n,

$$r_n=n^2/Z \ . \tag{27}$$

Taking r_n as a scaling parameter for the ion-surface distance D, one would emphasize that distance at which the ionic orbital just "touches" the surface.

Another possible choice is the classical threshold distance D_n, at which, in a one-dimensional picture, the top of the potential barrier between metal and ion (cf. Fig. 1) coincides with the ionic level with energy ϵ_n. This distance separates the range $D<D_n$, in which resonant electron transfer is classically allowed, from the classically forbidden range $D>D_n$. When D varies from very small to very large values, the qualitative behavior of the transition matrix elements and rates changes in the vicinity of $D=D_n$ from oscillatory to rapidly decreasing[26,35] (cf. also Fig. 2), i.e., D_n acts as a kind of "critical" parameter in the D dependence. We take this as our main argument for defining

$$D_s=D_n \ . \tag{28}$$

With this choice, the classical threshold distance is distinguished, in terms of the scaled distance $\tilde{D}$, by the value $\tilde{D}=1$. Disregarding the centrifugal potential for states with nonzero orbital angular momentum, we find the classical threshold distance for the Coulomb potential $V_c^>$ as

$$D_n=2n^2/Z\equiv 2r_n \ , \tag{29}$$

i.e., D_n differs from r_n by a constant factor only. Nevertheless, we adhere to the choice (28), the more so because it may be directly generalized to more general forms of the perturbing potential, including, for example, image-potential and angular momentum terms.

We now express the transition matrix elements in terms of the scaled parameters $\tilde{k}_\parallel$ and $\tilde{D}$. The "scaled representation" $\tilde{M}^{(Z)}_{nlm}(\tilde{k}_\parallel;\tilde{D})$ of the reduced matrix elements $M^{(Z)}_{nlm}(k_\parallel;D)$ is introduced as

$$\tilde{M}^{(Z)}_{nlm}(\tilde{k}_\parallel;\tilde{D})=M^{(Z)}_{nlm}(k_s\tilde{k}_\parallel;D_s\tilde{D})\equiv M^{(Z)}_{nlm}(\kappa_n\tilde{k}_\parallel;D_n\tilde{D}) \ . \tag{30}$$

Correspondingly, we define the scaled representation $\tilde{\mathcal{M}}^{(Z;V_0)}_{nlm}(\tilde{k}_\parallel;\tilde{D})$ of the full matrix elements $\mathcal{M}^{(Z;V_0)}_{nlm}(k_\parallel;D)$ [cf. Eq. (11) and (13); note that the scale transformation of $k_\parallel$ also affects the penetration coefficient b] by setting

$$\begin{aligned}\tilde{\mathcal{M}}^{(Z;V_0)}_{nlm}(\tilde{k}_\parallel;\tilde{D})&=\mathcal{M}^{(Z;V_0)}_{nlm}(k_s\tilde{k}_\parallel;D_s\tilde{D})\\&\equiv\mathcal{M}^{(Z;V_0)}_{nlm}(\kappa_n\tilde{k}_\parallel;D_n\tilde{D}) \ .\end{aligned} \tag{31}$$

In terms of the original (unscaled) parameters $k_\parallel$ and D, Eqs. (30) and (31) are written as

$$M^{(Z)}_{nlm}(k_\parallel;D)=\tilde{M}^{(Z)}_{nlm}(k_\parallel/k_s;D/D_s)\equiv\tilde{M}^{(Z)}_{nlm}(k_\parallel/\kappa_n;D/D_n) \tag{32}$$

and

$$\begin{aligned}\mathcal{M}^{(Z;V_0)}_{nlm}(k_\parallel;D)&=\tilde{\mathcal{M}}^{(Z;V_0)}_{nlm}(k_\parallel/k_s;D/D_s)\\&\equiv\tilde{\mathcal{M}}^{(Z;V_0)}_{nlm}(k_\parallel/\kappa_n;D/D_n) \ .\end{aligned} \tag{33}$$

It will be shown in Sec. IV A that for our choice of scaling parameters, the reduced transition matrix elements in scaled representation can be further reduced to a particularly simple form.

Turning now to the transition rates $\Gamma^{(Z;V_0)}_{nlm}(D)$, we define their representation with respect to the scaled ion-surface distance $\tilde{D}$ as

$$\tilde{\Gamma}^{(Z;V_0)}_{nlm}(\tilde{D})=\Gamma^{(Z;V_0)}_{nlm}(D_s\tilde{D})\equiv\Gamma^{(Z;V_0)}_{nlm}(D_n\tilde{D}) \tag{34}$$

or, equivalently

$$\Gamma^{(Z;V_0)}_{nlm}(D)=\tilde{\Gamma}^{(Z;V_0)}_{nlm}(D/D_s)\equiv\tilde{\Gamma}^{(Z;V_0)}_{nlm}(D/D_n) \ . \tag{35}$$

By changing in Eq. (23) the integration variable from $k_\parallel$ to $\tilde{k}_\parallel$ and using Eqs. (30) and (34), it follows that

$$\tilde{\Gamma}^{(Z;V_0)}_{nlm}(\tilde{D})=\frac{2}{\pi}\frac{\kappa_n^3}{V_0}\int_0^{\tilde{k}_n}d\tilde{k}_\parallel\tilde{k}_\parallel(\tilde{k}_n^2-\tilde{k}_\parallel^2)^{1/2}|\tilde{M}^{(Z)}_{nlm}(\tilde{k}_\parallel;\tilde{D})|^2, \tag{36}$$

where

$$\tilde{k}_n=k_n/\kappa_n\equiv(2V_0/\kappa_n^2-1)^{1/2} \tag{37}$$

is the (dimensionless) scaled jellium-electron momentum. In Sec. IV B, the expression (36) for the transition rate will be brought into a reduced form by exploiting properties of the reduced transition matrix elements and by using the potential depth V_0 as an additional scaling parameter.

IV. GENERAL ANALYSIS

In this section, we perform a general, formal analysis of the scaled representations of the transition matrix elements and rates. We make use of the defining expressions for the matrix elements and rates and, to some extent, of the closed-form expressions derived previously for the

matrix elements.[26] While the transition matrix elements are not the quantities of primary physical interest, a careful study of their properties is prerequisite to a systematic analysis of the transition rates.

A. Transition matrix elements

From Eqs. (12) and (30), we have explicitly

$$\tilde{M}^{(Z)}_{nlm}(\tilde{k}_\parallel;\tilde{D}) \equiv M^{(Z)}_{nlm}(k_s\tilde{k}_\parallel;D_s\tilde{D}) = \int d^3r[\chi^{(\kappa_n)}_{k_s\tilde{k}_\parallel}(\mathbf{r})]^* \left\{ \frac{-Z\Theta(z)}{|\mathbf{r}-D_s\tilde{D}\hat{\mathbf{e}}_z|} \right\} \times \psi^{(Z)}_{nlm}(\mathbf{r}-D_s\tilde{D}\hat{\mathbf{e}}_z) \quad (38)$$

(for the sake of argument, we keep the general notation k_s and D_s for the scaling parameters). Changing the integration variables to $\mathbf{r}'=\mathbf{r}/D_s$, we find

$$\tilde{M}^{(Z)}_{nlm}(\tilde{k}_\parallel;\tilde{D}) = D_s^2 \int d^3r'[\chi^{(\kappa_n)}_{k_s\tilde{k}_\parallel}(D_s\mathbf{r}')]^* \left\{ \frac{-Z\Theta(z')}{|\mathbf{r}'-\tilde{D}\hat{\mathbf{e}}_{z'}|} \right\} \times \psi^{(Z)}_{nlm}(D_s[\mathbf{r}'-\tilde{D}\hat{\mathbf{e}}_{z'}]) \; . \quad (39)$$

We note that the possibility to remove the D_s dependence from the perturbing potential is related to the fact that this potential is a homogeneous function of the coordinates.

To proceed further, we exploit scaling properties of the wave functions we have chosen to describe the initial and final states. From Eq. (A10), it is seen that for an arbitrary scaling parameter α,

$$\chi^{(\kappa_n)}_{k_\parallel}(\alpha\mathbf{r}) = \chi^{(\alpha\kappa_n)}_{\alpha k_\parallel}(\mathbf{r}) \; . \quad (40)$$

Exploiting the well-known scaling property of hydrogenic wave functions,[38]

$$\psi^{(Z)}_{nlm}(\beta\mathbf{r}) = \beta^{-3/2}\psi^{(\beta Z)}_{nlm}(\mathbf{r}) \; , \quad (41)$$

where β is an arbitrary scaling parameter, we then obtain from Eq. (39)

$$\tilde{M}^{(Z)}_{nlm}(\tilde{k}_\parallel;\tilde{D}) = D_s^{1/2} \int d^3r'[\chi^{(\kappa_n D_s)}_{k_s D_s \tilde{k}_\parallel}(\mathbf{r}')]^* \left\{ \frac{-Z\Theta(z')}{|\mathbf{r}'-\tilde{D}\hat{\mathbf{e}}_{z'}|} \right\} \times \psi^{(ZD_s)}_{nlm}(\mathbf{r}'-\tilde{D}\hat{\mathbf{e}}_{z'}) \; . \quad (42)$$

When forming the products $\kappa_n D_s$, $k_s D_s$, and ZD_s with our specific choice for the scaling parameters k_s and D_s, it turns out that they all are independent of Z:

$$\kappa_n D_s \equiv \kappa_n D_n = 2n \; , \quad (43)$$

$$k_s D_s \equiv \kappa_n D_n = 2n \; , \quad (44)$$

$$ZD_s \equiv ZD_n = 2n^2 \; . \quad (45)$$

Upon inserting these products into the expression (42) and combining the overall factors, we find that the reduced matrix element separates into the factor $Z^{1/2}$ and a Z-independent part:

$$\tilde{M}^{(Z)}_{nlm}(\tilde{k}_\parallel;\tilde{D}) = -(2Z)^{1/2} n \int d^3r'[\chi^{(2n)}_{2n\tilde{k}_\parallel}(\mathbf{r}')]^* \left\{ \frac{\Theta(z')}{|\mathbf{r}'-\tilde{D}\hat{\mathbf{e}}_{z'}|} \right\} \times \psi^{(2n^2)}_{nlm}(\mathbf{r}'-\tilde{D}\hat{\mathbf{e}}_{z'}) \; . \quad (46)$$

The separation property of the reduced matrix element holds for any choice of k_s and D_s that renders the products (43), (44), and (45) independent of Z. From a formal point of view, the simplest choice would be something like $k_s=Z$ and $D_s=1/Z$. A choice of this kind, however, could be hardly motivated on physical grounds and would not lead to the desired simplification in the description of resonant electron transfer.

We find it useful to rewrite Eq. (46) in the form

$$\tilde{M}^{(Z)}_{nlm}(\tilde{k}_\parallel;\tilde{D}) = \kappa_n^{1/2}\overline{M}_{nlm}(\tilde{k}_\parallel;\tilde{D}) \; , \quad (47)$$

with a *dimensionless*, "doubly reduced" matrix element

$$\overline{M}_{nlm}(\tilde{k}_\parallel;\tilde{D}) = -2^{1/2}n^{3/2} \int d^3r'[\chi^{(2n)}_{2n\tilde{k}_\parallel}(\mathbf{r}')]^* \left\{ \frac{\Theta(z')}{|\mathbf{r}'-\tilde{D}\hat{\mathbf{e}}_{z'}|} \right\} \times \psi^{(2n^2)}_{nlm}(\mathbf{r}'-\tilde{D}\hat{\mathbf{e}}_{z'}) \; . \quad (48)$$

This matrix element is independent of Z and V_0, i.e., independent of the parameters that characterize the strength of the ionic potential and the conduction-band potential, respectively. For a given set of ionic quantum numbers, it is a *universal* function of the scaled parameters $\tilde{k}_\parallel$ and $\tilde{D}$ (note that $\overline{M}_{nlm}$ is defined, as a function of $\tilde{k}_\parallel$, on the interval $0 \le \tilde{k}_\parallel < \infty$).

By introducing the scaled variables $\tilde{k}_\parallel$ and $\tilde{D}$ into the closed-form expressions for the transition matrix elements derived in Ref. 26, we also arrive at the factorized form (47) for the reduced matrix element, thereby obtaining a cross check for the scaling procedure. The resulting closed-form expression for the doubly reduced matrix element $\overline{M}_{nlm}(\tilde{k}_\parallel;\tilde{D})$ is given in compact form in Appendix B.

The full matrix element $\tilde{\mathcal{M}}^{(Z;V_0)}_{nlm}(\tilde{k}_\parallel;\tilde{D})$ is obtained from the doubly reduced matrix element $\overline{M}_{nlm}(\tilde{k}_\parallel;\tilde{D})$ by multiplication by the factor [cf. Eqs. (13), (47), and (A7)]

$$|b|\kappa_n^{1/2} \equiv \left[\frac{2}{V_0}(\tilde{k}_n^2-\tilde{k}_\parallel^2) \right]^{1/2} \kappa_n^{3/2} \quad (49)$$

(an irrelevant phase factor is omitted). The principal difference between the two matrix elements arises from the factor $(\tilde{k}_n^2-\tilde{k}_\parallel^2)^{1/2}$, which modifies the $\tilde{k}_\parallel$ dependence. As we deal in the following with the doubly reduced matrix elements only, we do not need to discuss this difference any further. Results of sample calculations of (squared) full transition matrix elements, both in unscaled and in scaled representation, can be found in Refs. 26,35,36.

In order to give a general impression of the shape of the doubly reduced matrix element, we display in Fig. 3 the squared matrix element $|\overline{M}_n(\tilde{k}_\parallel;\tilde{D})|^2$ (Ref. 46) for $n=8$ as a function of $\tilde{k}_\parallel$ and $\tilde{D}$. For $\tilde{k}_\parallel \ll 1$, the $\tilde{D}$

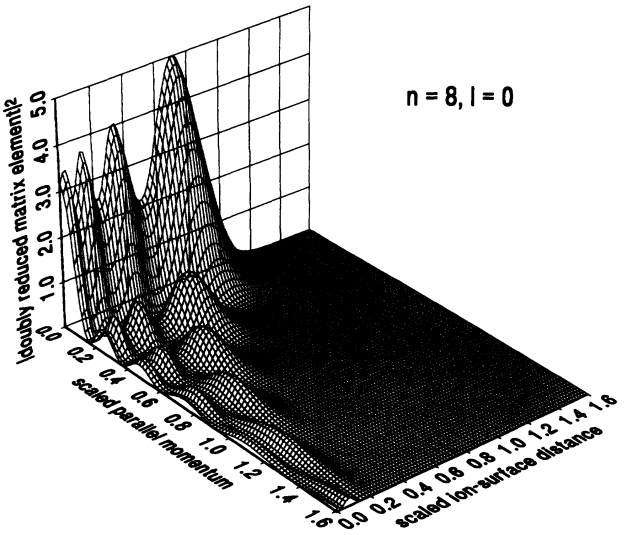

FIG. 3. Square modulus of the doubly reduced transition matrix element $\bar{M}_n$ for $n=8$, plotted as a function of the scaled parallel momentum $\tilde{k}_\parallel$ and the scaled ion-surface distance $\tilde{D}$.

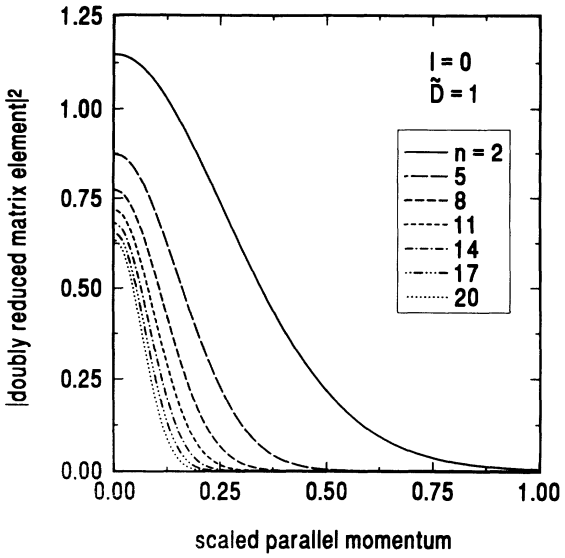

FIG. 4. Square modulus of the doubly reduced transition matrix elements $\bar{M}_n$ for $\tilde{D}=1$ and a sequence of n values, plotted as a function of the scaled parallel momentum $\tilde{k}_\parallel$.

dependence exhibits oscillatory structure that extends, with a roughly constant average value, out to the classical threshold distance $\tilde{D}=1$ (cf. also Fig. 2). Regarding the $\tilde{k}_\parallel$ dependence, it is seen that the matrix element becomes progressively more localized in the small-$\tilde{k}_\parallel$ range when $\tilde{D}$ increases. Qualitatively, this behavior is easily understood. At large ion-surface distances, the transition matrix element will be largest when the falloff of the jellium wave function with z is slowest. This requires the normal momentum component k_z to be maximum, i.e., the parallel component $k_\parallel$ to be minimum [cf. Eqs. (A2) and (A3)].

As shown in Appendix B, the extent of the squared $l=0$ matrix elements along the $\tilde{k}_\parallel$ axis can be roughly characterized, at not too small $\tilde{D}$, in terms of a width Δ_n that is proportional to $(n\tilde{D})^{-1/2}$ in the large-n limit. The results of sample calculations agree fairly well with this estimate (in the range $\tilde{D}<1$, a width can be assigned to the calculated matrix elements after averaging over the oscillatory structure). For our purposes, it is important that $\Delta_n \to 0$ when $n \to \infty$, i.e., the matrix elements tend to become more strongly localized in the small-$\tilde{k}_\parallel$ range when n gets larger. In order to illustrate this point, we display in Fig. 4 the $\tilde{k}_\parallel$ dependence of $|\bar{M}_n|^2$ at $\tilde{D}=1$ for a sequence of n values. By multiplying them with a common factor of about 1.5, the widths extracted from these curves can be brought into good agreement with the values for Δ_n derived from Eq. (B4).

The qualitative picture exhibited by Fig. 3 changes somewhat when $|\bar{M}_{nlm}(\tilde{k}_\parallel;\tilde{D})|^2$ is considered for nonzero quantum numbers l and m. Sample calculations have revealed (cf. also Figs. 12–15 of Ref. 26, where matrix elements corresponding to the full ionic Coulomb potential V_c are shown) that an increase of l at fixed n and $m=0$ entails an enhanced localization of the matrix element in the small-$\tilde{D}$ range, without substantial change of the localization along the $\tilde{k}_\parallel$ axis. This behavior can be qualitatively understood[7,26] in terms of the eccentricity of the classical electronic orbitals of the ion. Conversely, increasing m at fixed n and (large) l shifts the maximum of the matrix element to larger $\tilde{k}_\parallel$ values, leaving its localization in the small-$\tilde{D}$ range unaffected. This feature, which formally arises from the presence of the factor $\tilde{k}_\parallel^m$ in the matrix element (B1), may be interpreted in terms of the change in shape which the ionic wave functions undergo when m changes from small to large values.[14,26,47] However, if $n \to \infty$ at fixed l and m, the matrix element again becomes increasingly localized in the small $\tilde{k}_\parallel$ range.

B. Transition rates

With the form (47) of the reduced transition matrix element in scaled representation, we obtain from Eq. (36),

$$\tilde{\Gamma}_{nlm}^{(Z;V_0)}(\tilde{D})=\frac{2}{\pi}\frac{\kappa_n^4}{V_0}\int_0^{\tilde{k}_n} d\tilde{k}_\parallel \tilde{k}_\parallel (\tilde{k}_n^2-\tilde{k}_\parallel^2)^{1/2} \times |\bar{M}_{nlm}(\tilde{k}_\parallel;\tilde{D})|^2 . \quad (50)$$

This expression can be further reduced by using the potential depth V_0 as a scaling parameter, in terms of which quantities having dimension of an energy are scaled.[48]

We define the (dimensionless) scaled binding energy of the ionic orbital with principal quantum number n as

$$\tilde{\delta}_n=|\epsilon_n|/V_0\equiv\kappa_n^2/2V_0 , \quad (51)$$

so that $0<\tilde{\delta}_n<1$ for resonant electron transfer into bound conduction-band states. Further, as we use atomic units and therefore have dimensional equivalence of quantities having dimension of an energy and dimension of a reciprocal time, we can write the transition rate (or

decay width) $\tilde{\Gamma}_{nlm}^{(Z;V_0)}(\tilde{D})$ in terms of a dimensionless, reduced transition rate (or reduced decay width) $\bar{\Gamma}_{nlm}^{(Z;V_0)}(\tilde{D})$ as

$$\tilde{\Gamma}_{nlm}^{(Z;V_0)}(\tilde{D})=V_0\bar{\Gamma}_{nlm}^{(Z;V_0)}(\tilde{D}) . \tag{52}$$

The reduced transition rate introduced here is to be distinguished from the reduced rate defined in Ref. 36 for the specific case $l=0$.

From Eqs. (50)–(52), we find that $\bar{\Gamma}_{nlm}^{(Z;V_0)}(\tilde{D})$ depends on Z and V_0 through the scaled binding energy $\tilde{\delta}_n$ only,

$$\bar{\Gamma}_{nlm}^{(Z;V_0)}(\tilde{D})\equiv\bar{\Gamma}_{nlm}^{(\tilde{\delta}_n)}(\tilde{D}) =\frac{8}{\pi}\tilde{\delta}_n^2\int_0^{\tilde{k}_n}d\tilde{k}_\parallel f(\tilde{k}_\parallel;\tilde{k}_n)|\bar{M}_{nlm}(\tilde{k}_\parallel;\tilde{D})|^2 \tag{53}$$

where now

$$\tilde{k}_n=(1/\tilde{\delta}_n-1)^{1/2} \tag{54}$$

from Eqs. (37) and (51), and the weight function

$$f(\tilde{k}_\parallel;\tilde{k}_n)=\tilde{k}_\parallel(\tilde{k}_n^2-\tilde{k}_\parallel^2)^{1/2} \tag{55}$$

attains its maximum at $\tilde{k}_\parallel=\tilde{k}_n/\sqrt{2}$. The full transition rate $\Gamma_{nlm}^{(Z;V_0)}(D)$ defined by Eq. (23) is expressed in terms of $\bar{\Gamma}_{nlm}^{(\tilde{\delta}_n)}(\tilde{D})$ by using Eqs. (35), (52), and (53). At this point, it should be noted that the formal development leading to Eq. (53) for the reduced transition rate has been, within our model assumptions, completely general and does not imply any approximations.

The qualitative behavior of the reduced transition rate $\bar{\Gamma}_{nlm}^{(\tilde{\delta}_n)}(\tilde{D})$ as a function of its parameters is determined by the overlap of the weight function $f(\tilde{k}_\parallel;\tilde{k}_n)$ with the squared matrix element $|\bar{M}_{nlm}(\tilde{k}_\parallel;\tilde{D})|^2$ in the integration interval $0\le\tilde{k}_\parallel\le\tilde{k}_n$. We do not enter a general discussion of this matter, but confine ourselves to the cases that are of interest to the present study.

In Sec. V, we will analyze transition matrix elements and rates in the limit of large principal quantum numbers n at fixed values of the angular momentum quantum numbers l and m (in particular, at $l=0$). As discussed in Sec. IV A, the matrix elements $\bar{M}_{nlm}(\tilde{k}_\parallel;\tilde{D})$ for $\tilde{D}>0$ become, in the large-n limit, increasingly localized in the small-$\tilde{k}_\parallel$ range. Therefore, if n is chosen (at fixed, nonzero $\tilde{D}$) to be sufficiently large, sizable contributions to the integral in Eq. (53) will arise only from an arbitrarily small vicinity of the point $\tilde{k}_\parallel=0$. Then, if the parameter $\tilde{k}_n$ approaches a constant value in the large-n limit, or increases with n, we can approximate the second factor in the weight function (55) as

$$(\tilde{k}_n^2-\tilde{k}_\parallel^2)^{1/2}\approx\tilde{k}_n\approx\tilde{\delta}_n^{-1/2} . \tag{56}$$

From Eq. (54), it is easily seen that the condition on $\tilde{k}_n$ is fulfilled particularly in two specific cases, viz., that of fixed Z and that of fixed $\kappa_n\equiv Z/n$. In the first case, we have $\tilde{k}_n\propto n$ in the large-n limit; in the second case, $\tilde{k}_n=$const.

The case of fixed Z and varying, large n is realized, e.g., in resonance ionization of atomic Rydberg states,[14] for which $Z\approx 1$. In the case of fixed κ_n, we consider transition rates at different Z values, but at one and the same value of the electronic energy. We encounter this case, e.g., in the treatment of resonance neutralization of highly charged ions, in which successive transfer of metal electrons with energy close to the Fermi energy entails a successive change of the effective ion core charge.[7]

Now, by using Eq. (56) and replacing in the integral of Eq. (53) the upper integration limit with ∞, we can write the reduced transition rate $\bar{\Gamma}_{nlm}^{(\tilde{\delta}_n)}(\tilde{D})$ for arbitrary n in the approximate form

$$\bar{\Gamma}_{nlm}^{(\tilde{\delta}_n)}(\tilde{D})=\frac{8}{\pi}\tilde{\delta}_n^{3/2}\gamma_{nlm}(\tilde{D}) . \tag{57}$$

The dimensionless, doubly reduced transition rate $\gamma_{nlm}(\tilde{D})$ defined as

$$\gamma_{nlm}(\tilde{D})=\int_0^\infty d\tilde{k}_\parallel\tilde{k}_\parallel|\bar{M}_{nlm}(\tilde{k}_\parallel;\tilde{D})|^2 \equiv\tfrac{1}{2}\int_0^\infty d\chi|\bar{M}_{nlm}(\sqrt{\chi};\tilde{D})|^2 \tag{58}$$

is independent of Z and V_0. For given ionic quantum numbers, it is a *universal* function of $\tilde{D}$. Equation (57) is supposed to become an exact relation in the limit $n\to\infty$. The factorized form of $\bar{\Gamma}_{nlm}^{(\tilde{\delta}_n)}(\tilde{D})$ bears a resemblance to the factorized form (47) of the reduced transition matrix element $\bar{M}_{nlm}^{(Z)}(\tilde{k}_\parallel;\tilde{D})$, which, however, holds exactly for arbitrary n,l,m.

The convergence behavior in Eq. (57) is expected to be qualitatively different, depending on whether Z or κ_n is kept fixed. In the former case, we have $\tilde{k}_n\to\infty$ for $n\to\infty$, so that convergence requires only the existence of a fixed (n-independent) cutoff value of $\tilde{k}_\parallel$ beyond which the matrix elements effectively vanish. The approximate $n^{-1/2}$ dependence of the actual cutoff [cf. Eq. (B4)] accelerates the convergence. For fixed κ_n, where $\tilde{k}_n=$const, convergence is achieved only through the $n^{-1/2}$ dependence of the cutoff. So we expect in this case a much slower convergence than in the case of fixed Z.

In Fig. 5, we show the $\tilde{D}$ dependence of the doubly re-

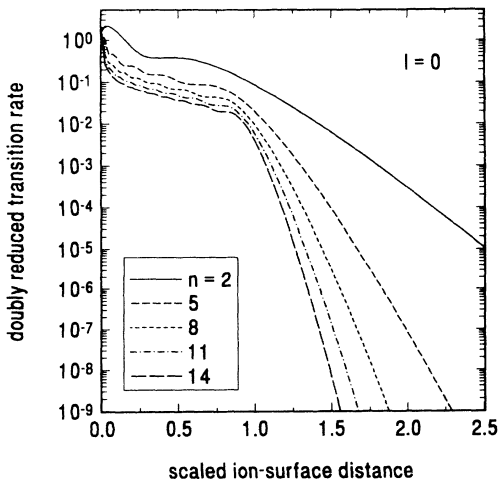

FIG. 5. Doubly reduced transition rates γ_n for a sequence of n values, plotted as a function of the scaled ion-surface distance $\tilde{D}$.

duced transition rate $\gamma_n(\tilde{D})$[46] for a sequence of n values. The qualitative behavior of the curves is, of course, compatible with that observed in previous calculations of the full transition rate (36).[14,35,36,47] We note that, contrary to the behavior of the transition matrix elements at $\tilde{k}_{\parallel}=0$ (cf. Figs. 3 and 7 below), the $\tilde{D}$-averaged rates in the range $\tilde{D}<1$ do not exhibit a more or less constant value, but decrease by about one order of magnitude when $\tilde{D}$ varies from zero to unity. This behavior apparently reflects the increasing localization of the matrix elements in the small-$\tilde{k}_{\parallel}$ range, as expressed by the $\tilde{D}^{-1/2}$ dependence of the width Δ_n. At $\tilde{D}=0$, the rates γ_n are found to be independent of n,

$$\gamma_n(0)=\frac{\pi}{2}\ , \tag{59}$$

within the accuracy of the numerical calculation [cf. also Eqs. (B5) and (B6)].

Using Eqs. (52) and (57) along with the results of Fig. 5, we can generate approximate transition rates for specific parameter values, which may be compared to rates calculated exactly from Eq. (50). In Fig. 6, exact and approximate rates are compared for $n=5$, $l=0$, and $V_0=0.5$ a.u. The Z values are chosen so as to correspond to an atomic Rydberg state ($Z=1$) and to an ionic state with energy in the vicinity of the Fermi level of a typical metal ($Z=3.125$; this value corresponds to the κ_n value used in the calculations of Ref. 35), respectively. As is to be expected from the discussion above, the agreement between exact and approximate results is much better for $Z=1$ than for $Z=3.125$. With increasing $\tilde{D}$, the agreement becomes closer, in conformity with what one anticipates from the localization properties of the transition matrix elements [cf. Eq. (B4)].

From Eq. (57), the transition rates for a Rydberg series

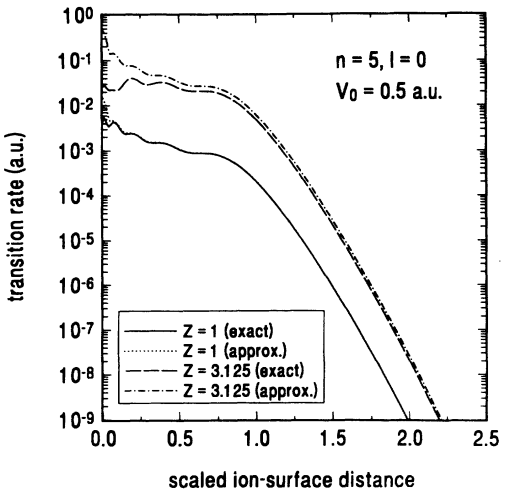

FIG. 6. Transition rates $\tilde{\Gamma}_n^{(Z;V_0)}$ for the indicated parameter values, plotted as a function of the scaled ion-surface distance $\tilde{D}$. The curves labelled "exact" refer to the direct evaluation of Eq. (50), the approximate curves to a calculation using Eqs. (52) and (57).

of atomic states at fixed Z are seen to be suppressed, in comparison with the rates for fixed κ_n, by a factor n^{-3}. This feature appears to result qualitatively from the increasing mismatch in linear momentum, which occurs between the initial and final states when their binding energy goes to zero.

V. LARGE-n LIMIT AND SCALING LAWS

The formal analysis of the preceding section has shown that, within our model, transition matrix elements and rates in scaled representation can be expressed essentially in terms of reduced, universal functions which do not depend on the parameters characterizing the electronic potentials in the ion-metal system. In the following, we will achieve a further reduction by systematically analyzing the limit of large ionic principal quantum numbers n. This enables us, in particular, to establish scaling laws that connect transition matrix elements and rates for different (finite) values of the principal quantum number. In the analysis, we combine the results of Sec. IV with the evidence derived from explicit numerical calculations. A purely formal examination of the large-n limit, based solely on manipulating closed-form expressions, is inhibited by mathematical intricacies.

In our previous analyses of the large-n behavior of resonant-electron transfer,[35,36] we had chosen as our starting point, somewhat arbitrarily, sequences of calculated transition matrix elements for $\tilde{k}_{\parallel}=0$. Here, this choice appears to be simply a consequence of the strong localization of the matrix elements in the vicinity of $\tilde{k}_{\parallel}=0$, which we have elaborated upon in Sec. IV. This localization suggests that the scaling properties of the transition rates in the large-n limit bear similarities to those of the $\tilde{k}_{\parallel}=0$ matrix elements.

Throughout this section, we will consider the case $l=0$ only. This is consistent with the neglect of angular momentum effects in the definition of the scaling parameter D_s. We will briefly comment on the case $l>0$ in Sec. VI.

A. Transition matrix elements

In Fig. 7, doubly reduced matrix elements $|\bar{M}_n|^2$ (Ref. 46) for $\tilde{k}_{\parallel}=0$ are shown as a function of $\tilde{D}$ for a sequence of n values. In the range $\tilde{D}<1$, the curves are seen to oscillate about an approximately constant average value and acquire the common value π at $\tilde{D}=0$ [cf. Eq. (B6)]. A notable feature, which requires a little more analysis, is the near coincidence of the values of the matrix elements at the classical threshold $\tilde{D}=1$.

In Fig. 8, values of $|\bar{M}_n(0;1)|^2$ are shown for n values up to 40. We interpret the progressively slower decrease with n as an indication for convergence of the matrix elements towards a nonzero limiting value:

$$\lim_{n\to\infty}|\bar{M}_n(0;1)|^2=|\bar{M}_\infty(0;1)|^2>0\ . \tag{60}$$

An extrapolation of the values of Fig. 8 gives $|\bar{M}_\infty(0;1)|^2\approx 0.55$. From the numerical calculation, we cannot exclude, of course, the possibility of a weak falloff

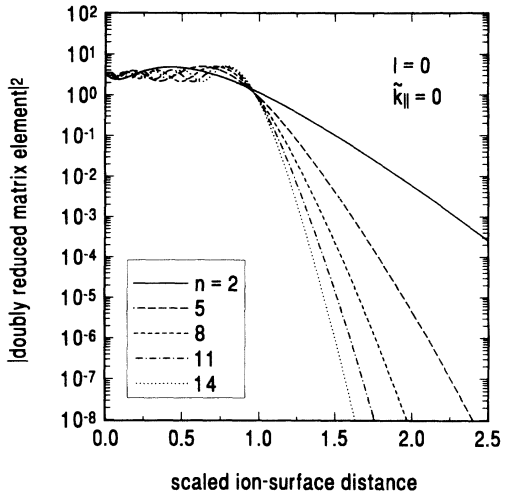

FIG. 7. Square modulus of the doubly reduced transition matrix elements $\bar{M}_n$ for $\tilde{k}_\parallel=0$ and a sequence of n values, plotted as a function of the scaled ion-surface distance $\tilde{D}$.

persisting even at asymptotically large n values. However, when multiplying the calculated squared matrix elements by $\ln n$, we find that the resulting values continue to increase with increasing n (cf. Fig. 8). We therefore conclude that even a logarithmic falloff is unlikely to occur asymptotically. We note that an analytic evaluation of $\bar{M}_n(0;1)$ from the closed-form expression (B1), particularly in the large-n limit, has not been achieved.

1. *The classically forbidden range*

Universal behavior of the matrix elements in the large-n limit is most easily revealed by first analyzing the classically forbidden range $\tilde{D}>1$. It is seen from Fig. 7 that the *ratios* of squared matrix elements corresponding to adjacent curves (i.e., to n values differing by three units) are, for fixed $\tilde{D}>1$, largely independent of n. For quantitative analysis of this behavior, we consider ratios of squared matrix elements for adjacent n values, i.e., for n values differing by one unit. In Fig. 9, calculated ratios are shown for a sequence of pairs of n values with n up to 20. The ratios are seen to converge rapidly towards a limiting function, so that we may write

$$\lim_{n\to\infty}|\bar{M}_n(0;\tilde{D})/\bar{M}_{n-1}(0;\tilde{D})|^2=\Xi(\tilde{D}),\quad \tilde{D}\geq 1\ . \tag{61}$$

The dimensionless function $\Xi(\tilde{D})$ is a *universal* (n independent) function of $\tilde{D}$ satisfying, in conformity with Eq. (60), $\Xi(1)=1$. From the definition of the doubly reduced matrix elements $\bar{M}_n(\tilde{k}_\parallel;\tilde{D})$, it follows that $\Xi(\tilde{D})$ is identical to the function $f(\tilde{D})$ introduced in Ref. 35 in the analysis of the full matrix elements $\bar{\mathcal{M}}_n(0;\tilde{D})$ for fixed κ_n, and identical to the function $\Xi(\tilde{D})$ introduced in Ref. 36.

We have not managed to obtain a closed-form representation for $\Xi(\tilde{D})$, but the uppermost of the (thick) curves in Fig. 9 ($n=20/n=19$) is supposed to give a very good numerical approximation to this function. In the range of asymptotically large ion-surface distances, $\tilde{D}\gg 1$, we obtain, by keeping in Eq. (B1) the leading-order term ($\tau=0$) only and taking the limit $n\to\infty$,

$$\Xi(\tilde{D})\approx 16\tilde{D}^2\exp(2-4\tilde{D})=118.2\tilde{D}^2\exp(-4\tilde{D}),\quad \tilde{D}\gg 1\ . \tag{62}$$

This approximation to $\Xi(\tilde{D})$ is shown in Fig. 9 as a thin, long-dashed curve.

In view of the rapid, monotonic convergence of the matrix-element ratios towards the limiting function

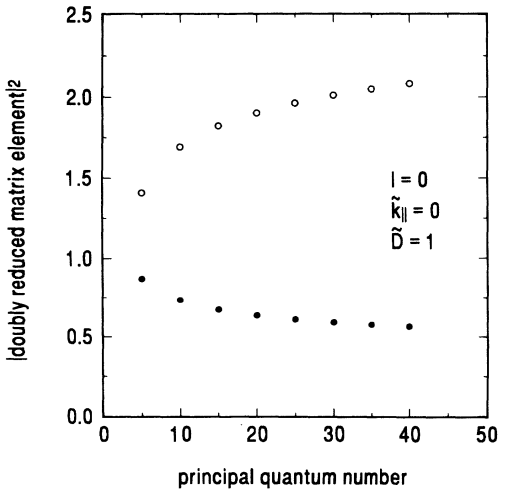

FIG. 8. Solid circles: square modulus of the doubly reduced transition matrix element $\bar{M}_n$ for $\tilde{k}_\parallel=0$ and $\tilde{D}=1$, plotted as a function of the principal quantum number n. Empty circles: values given by the solid circles, multiplied by $\ln n$.

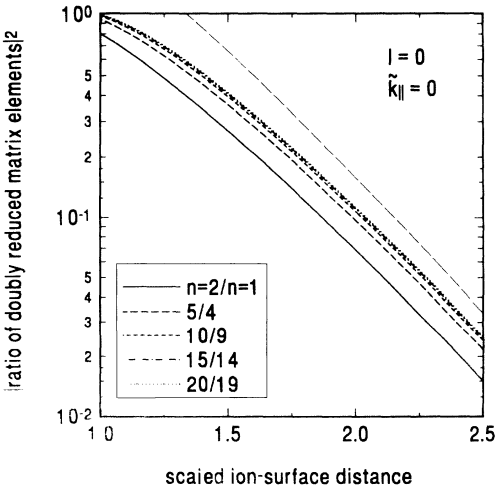

FIG. 9. Square modulus of ratios of doubly reduced transition matrix elements $\bar{M}_n$ for $\tilde{k}_\parallel=0$ and a sequence of pairs of adjacent n values, plotted as a function of the scaled ion-surface distance $\tilde{D}$. The thin, long-dashed line corresponds to the asymptotic approximation (62) to the function $\Xi(\tilde{D})$.

$\Xi(\tilde{D})$, we may now use Eq. (61) as an approximate relation for finite principal quantum numbers n. Be repeated application of this relation, we can write, for arbitrary principal quantum numbers n_1 and n_2,

$$|\bar{M}_{n_1}(0;\tilde{D})|^2=[\Xi(\tilde{D})]^{n_1-n_2}|\bar{M}_{n_2}(0;\tilde{D})|^2, \quad \tilde{D}\geq 1 , \tag{63}$$

thereby establishing a *scaling law* for the doubly reduced transition matrix elements at $\tilde{k}_{\parallel}=0$.

Using Eq. (13), (30), (47), and (63), we can immediately write down scaling laws for the full matrix elements given by Eq. (11). In doing so, we distinguish the cases of fixed ion core charge Z and of fixed κ_n (cf. Sec. IV B). In the former case, the penetration coefficient b attains a constant limiting value when $n\to\infty$, while in the latter case it is independent of n. The only difference between the two cases then comes about through the factor $\kappa_n^{1/2}$ in Eq. (47), so that we obtain

$$|\tilde{\mathcal{M}}^{[Z]}_{n_1}(0;\tilde{D})|^2=\frac{n_2}{n_1}[\Xi(\tilde{D})]^{n_1-n_2}|\tilde{\mathcal{M}}^{[Z]}_{n_2}(0;\tilde{D})|^2, \quad \tilde{D}\geq 1 \tag{64}$$

for fixed Z (superscript "$[Z]$") and

$$|\tilde{\mathcal{M}}^{[\epsilon]}_{n_1}(0;\tilde{D})|^2=[\Xi(\tilde{D})]^{n_1-n_2}|\tilde{\mathcal{M}}^{[\epsilon]}_{n_2}(0;\tilde{D})|^2, \quad \tilde{D}\geq 1 \tag{65}$$

for fixed κ_n, i.e., for fixed electronic energy (superscript "$[\epsilon]$"). By using Eqs. (29), (31), and (33), we can transform these relations back to the "unscaled" representation in terms of the ion-surface distance D:

$$|\mathcal{M}^{[Z]}_{n_1}(0;D)|^2=\frac{n_2}{n_1}[\Xi(D/D_{n_1})]^{n_1-n_2} \times|\mathcal{M}^{[Z]}_{n_2}(0;n_2^2D/n_1^2)|^2, \quad D\geq D_{n_1} \tag{66}$$

and

$$|\mathcal{M}^{[\epsilon]}_{n_1}(0;D)|^2=[\Xi(D/D_{n_1})]^{n_1-n_2}|\mathcal{M}^{[\epsilon]}_{n_2}(0;n_2D/n_1)|^2 , \quad D\geq D_{n_1} \tag{67}$$

(the different powers of n_2/n_1 in the arguments of $\mathcal{M}^{[Z]}_{n_2}$ and $\mathcal{M}^{[\epsilon]}_{n_2}$ arise from the difference in the ratio D_{n_2}/D_{n_1} for the two cases).

The scaling law (63) and its specific forms (64)–(67) are *approximate* relations that may be used to generate matrix elements with arbitrary quantum number n_1 from the function $\Xi(\tilde{D})$ and a single, known matrix element with quantum number n_2. The error made when applying this procedure apparently decreases with increasing n_2 if n_1-n_2 is kept fixed, and with decreasing n_1-n_2 if n_2 is kept fixed. For $n_1>n_2\geq 10$, the order of magnitude of the error is estimated from the curves of Fig. 9 to be less than 10%.

2. *The classically allowed range*

It is appropriate to ask whether scaling laws similar to those obtained for the transition matrix elements in the range $\tilde{D}>1$ can be established also in the classically allowed range $\tilde{D}<1$. An immediate extension of Eq. (61) appears to be not feasible. The oscillating character of the matrix elements for $\tilde{D}<1$ (cf. Fig. 7) is likely to inhibit the convergence of their ratios towards a universal limiting function. However, details of the oscillatory structure are not expected to play a significant role in the dynamics of resonant-electron transfer, the more so since orthogonalization of the initial and final states (cf. Sec. II C) tends to smooth out this structure. We therefore consider *average* values of the squared matrix elements with respect to $\tilde{D}$.

Without performing the averaging explicitly, we infer from calculations like the one shown in Fig. 7 that, except for the vicinity of $\tilde{D}=1$, the $\tilde{D}$-averaged values of the squared matrix elements, $\overline{|\bar{M}_n(0;\tilde{D})|^2}$ stay close to the common value which the unaveraged matrix elements attain at $\tilde{D}=0$:

$$\overline{|\bar{M}_n(0;\tilde{D})|^2}\approx\pi, \quad \tilde{D}<1 \tag{68}$$

[cf. Eq. (B6)]. In order to deal with the vicinity of $\tilde{D}=1$, we derive from Eq. (63) scaling laws that allow a smooth continuation across this point.

Let us assume Eq. (63) to be written down twice, for pairs of principal quantum numbers n_1,n_2 and n_3,n_4, respectively. By eliminating the function $\Xi(\tilde{D})$ from the resulting equations, we find

$$|\bar{M}_{n_1}(0;\tilde{D})|^2=\left|\frac{\bar{M}_{n_3}(0;\tilde{D})}{\bar{M}_{n_4}(0;\tilde{D})}\right|^{2n_{12}/n_{34}}|\bar{M}_{n_2}(0;\tilde{D})|^2 , \tag{69}$$

where $n_{ij}=n_i-n_j$. Specializing to the case $n_2=n_3$ and changing notation, we can write in particular

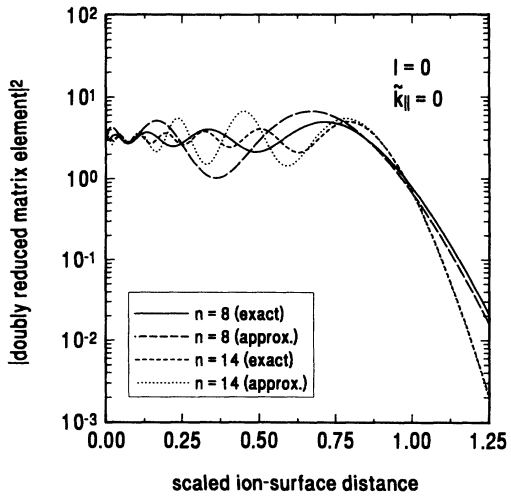

FIG. 10. Square modulus of doubly reduced transition matrix elements $\bar{M}_n$ for $\tilde{k}_{\parallel}=0$ and $n=8,14$, plotted as a function of the scaled ion-surface distance $\tilde{D}$. The curves labeled "approx." correspond to the approximate evaluation of the matrix elements from the relation (70), with $n_2=5$, $n_3=2$ for $n=8$, and $n_2=11$, $n_3=8$ for $n=14$.

$$|\overline{M}_{n_1}(0;\tilde{D})|^2=\frac{|\overline{M}_{n_2}(0;\tilde{D})|^{2n_{13}/n_{23}}}{|\overline{M}_{n_3}(0;\tilde{D})|^{2n_{12}/n_{23}}} . \quad (70)$$

As the matrix elements are defined in the range $0\le\tilde{D}<\infty$, the scaling laws (69) and (70) are formally defined also for $\tilde{D}<1$ and, in this respect, are more general than Eq. (63). When these laws are applied in an approximate calculation of transition matrix elements in the range $\tilde{D}>1$, knowledge of at least two matrix elements for different n values, instead of one matrix element and the function $\Xi(\tilde{D})$, is required. However, if matrix elements with n values close to that of the element to be calculated are available, Eqs. (69) and (70) may be more accurate than Eq. (63). The transformation of Eqs. (69) and (70) to the unscaled representation is obvious and will not be carried out here.

In order to illustrate the suitability of Eq. (70), we compare in Fig. 10 matrix elements for $n=8$ and $n=14$ evaluated from this equation to the exact matrix elements (cf. Fig. 7). The exact $n=2$ and $n=5$ ($n=8$ and $n=11$) matrix elements have been used as input to calculate the $n=8$ ($n=14$) matrix element. The good agreement observed for $\tilde{D}>1$ persists in the range $\tilde{D}<1$, until the phase difference between the oscillations in the exact and approximate matrix elements becomes too large. We note that with the approximation (68), the average values $|\overline{M}_n(0;\tilde{D})|^2$ trivially fulfill Eqs. (69) and (70).

3. *The case* $\tilde{k}_\parallel>0$

By continuity arguments, the scaling laws for $\tilde{k}_\parallel=0$ are expected to hold, to a certain degree of accuracy, also for $\tilde{k}_\parallel>0$. In Fig. 11, we show the $\tilde{D}$ dependence of $|\overline{M}_n(\tilde{k}_\parallel;\tilde{D})|^2$ for various pairs of adjacent n values and a number of $\tilde{k}_\parallel$ values. For $\tilde{k}_\parallel\ll1$, the ratios deviate by less than 10% from the universal function $\Xi(\tilde{D})$ derived for $\tilde{k}_\parallel=0$ and $n\to\infty$. With increasing $\tilde{k}_\parallel$, the deviations tend to become larger, particularly in the vicinity of $\tilde{D}=1$, where the ratios start to exhibit oscillatory behavior. Nevertheless, for sufficiently small $\tilde{k}_\parallel$, we can generalize the relation (63) by writing

$$|\overline{M}_{n_1}(\tilde{k}_\parallel;\tilde{D})|^2=[\Xi(\tilde{D})]^{n_1-n_2}|\overline{M}_{n_2}(\tilde{k}_\parallel;\tilde{D})|^2 ,$$
$$\tilde{k}_\parallel\ll1,\quad \tilde{D}\ge1 . \quad (71)$$

Correspondingly, the relations (64)–(67), (69), and (70) can also be extended into the range $0<\tilde{k}_\parallel\ll1$.

B. Transition rates

Following closely the procedure pursued for the transition matrix elements, we now analyze scaling properties of the transition rates in the large-n limit. We consider the doubly reduced transition rate $\gamma_n(\tilde{D})$ defined by Eq. (58). According to the discussion of Sec. IV B, the integrand in this equation is localized, in the large-n limit, in the immediate vicinity of $\tilde{k}_\parallel=0$. However, it would be premature to conclude therefrom that, for *finite* principal quantum numbers n, the scaling properties of the rates $\gamma_n(\tilde{D})$ are necessarily identical to those of the squared matrix elements $|\overline{M}_n(0;\tilde{D})|^2$. Rather, we have to study explicitly the effect of the $\tilde{k}_\parallel$ integration in Eq. (58) at finite, fixed n.

We start from the observation that, unlike the $\tilde{k}_\parallel=0$ matrix elements shown in Fig. 7, the doubly reduced transition rates of Fig. 5 exhibit a rapid decrease with n at the classical threshold $\tilde{D}=1$. In order to analyze this feature, we display in Fig. 12 the values of $\gamma_n(1)$ for a sequence of n values ranging from 1 to 20 in a log-log plot. For large n, the calculated values are seen to follow closely the straight line, which corresponds to an exact $n^{-3/2}$ dependence. The appearance of a simple power law for

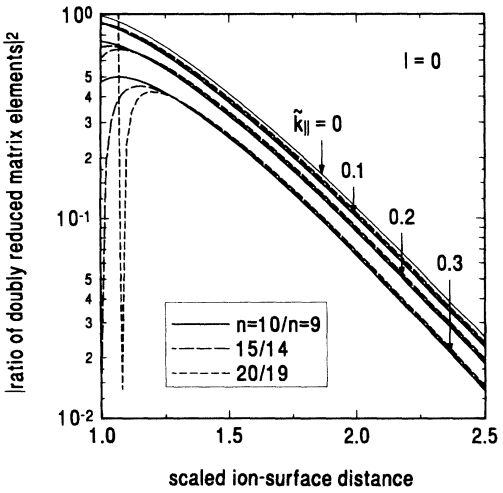

FIG. 11. Square modulus of ratios of doubly reduced transition matrix elements $\overline{M}_n$ for various $\tilde{k}_\parallel$ values and pairs of adjacent n values, plotted as a function of the scaled ion-surface distance $\tilde{D}$. The thin solid curve corresponds to the universal function $\Xi(\tilde{D})$ introduced in Eq. (61).

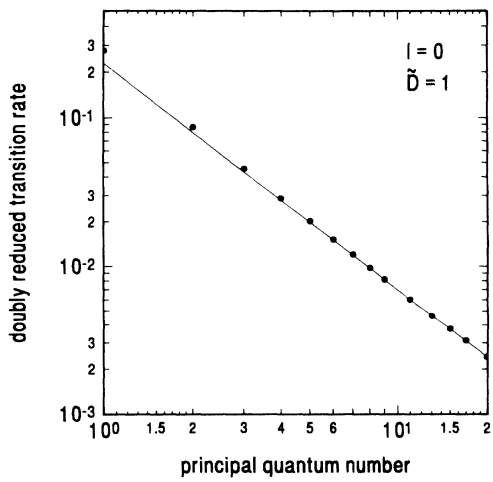

FIG. 12. Doubly reduced transition rate γ_n at $\tilde{D}=1$, plotted as a function of the ionic principal quantum number n. The solid straight line, which has been adjusted to the calculated values at $n=20$, corresponds to an exact $n^{-3/2}$ dependence.

the n dependence of $\gamma_n(1)$, in particular with a half-integer exponent, is a surprising result, for which we are not able to present a formal proof. We note that a power $n^{-3/2}$ shows up as an overall factor in the large-n approximants to the hydrogenic wave functions.[38] This factor may provide a formal explanation for the overall factor n^{-3} in the reduced transition rate (57), but obviously cannot be related to the occurrence of a power $n^{-3/2}$ in the doubly reduced rate.

Now, by writing for arbitrary $\tilde{D}$,

$$\gamma_n(\tilde{D})=n^{-3/2}\bar{\gamma}_n(\tilde{D}) , \tag{72}$$

we introduce "triply reduced" transition rates $\bar{\gamma}_n(\tilde{D})$. In view of the evidence expressed by Fig. 12, we suppose these rates to converge, at $\tilde{D}=1$, towards a nonzero limiting value when $n\to\infty$:

$$\lim_{n\to\infty}\bar{\gamma}_n(1)=\bar{\gamma}_\infty(1)>0 . \tag{73}$$

This relation parallels the relation (60) for the $\tilde{k}_\parallel=0$ transition matrix elements. From extrapolating the calculated values for $\gamma_n(1)$ shown in Fig. 12, we find $\bar{\gamma}_\infty(1)\approx 0.22$.

1. *The classically forbidden range*

In the range $\tilde{D}>1$, we analyze ratios of triply reduced transition rates for pairs of adjacent n values. In Fig. 13, these ratios are displayed for those n-values for which ratios of $\tilde{k}_\parallel=0$ transition matrix elements were shown in Fig. 9. The ratios of the rates are seen to exhibit, with increasing n, monotonic convergence towards a limiting function. If we take the curve for $n=20/n=19$ to represent this function, we find that its values are consistently larger by about 1% than those of the corresponding curve in Fig. 9. Yet it is plausible to assume that the ratios of the rates $\bar{\gamma}_n(\tilde{D})$ converge precisely towards the universal function $\Xi(\tilde{D})$, which determines the limit of the ratios of the squared matrix elements $|\bar{M}_n(0;\tilde{D})|^2$. We therefore write

$$\lim_{n\to\infty}[\bar{\gamma}_n(\tilde{D})/\bar{\gamma}_{n-1}(\tilde{D})]=\Xi(\tilde{D}),\quad \tilde{D}\geq 1 . \tag{74}$$

The difference between the uppermost curves of Figs. 9 and 13 is ascribed to a faster convergence of the ratios of the transition rates, in comparison with the ratios of the transition matrix elements, towards $\Xi(\tilde{D})$. Consequently, we suppose the curve for the rates to give an even better numerical approximation to $\Xi(\tilde{D})$ than does the curve for the matrix elements.

A faster convergence of the ratios of the triply reduced transition rates is anticipated already from a comparison of the large-n behavior of transition matrix elements and rates at $\tilde{D}=1$ (cf. Figs. 8 and 12). The rates approach their asymptotic $n^{-3/2}$ dependence much faster than the matrix elements approach their constant limiting value. We note that, since $\lim_{n\to\infty}[n/(n-1)]^{3/2}=1$, the relation (74) is formally fulfilled also for the doubly reduced transition rates $\gamma_n(\tilde{D})$. With these rates, however, the convergence in Eq. (74) would be very slow.

Using Eq. (74) as an approximate relation for finite n, we can now immediately write down *scaling laws* for the transition rates, which bear a close resemblance to the scaling laws (63)–(69) for the $\tilde{k}_\parallel=0$ transition matrix elements.

For arbitrary principal quantum numbers n_1 and n_2, we obtain, in analogy to Eq. (63),

$$\bar{\gamma}_{n_1}(\tilde{D})=[\Xi(\tilde{D})]^{n_1-n_2}\bar{\gamma}_{n_2}(\tilde{D}),\quad \tilde{D}\geq 1 . \tag{75}$$

Using Eq. (72), we then have

$$\gamma_{n_1}(\tilde{D})=\left[\frac{n_2}{n_1}\right]^{3/2}[\Xi(\tilde{D})]^{n_1-n_2}\gamma_{n_2}(\tilde{D}),\quad \tilde{D}\geq 1 . \tag{76}$$

For the full transition rates in scaled representation, we find, by using Eqs. (52), (57), and (72),

$$\tilde{\Gamma}^{[Z]}_{n_1}(\tilde{D})=\left[\frac{n_2}{n_1}\right]^{9/2}[\Xi(\tilde{D})]^{n_1-n_2}\tilde{\Gamma}^{[Z]}_{n_2}(\tilde{D}),\quad \tilde{D}\geq 1 \tag{77}$$

for fixed ion core charge Z, and

$$\tilde{\Gamma}^{[\epsilon]}_{n_1}(\tilde{D})=\left[\frac{n_2}{n_1}\right]^{3/2}[\Xi(\tilde{D})]^{n_1-n_2}\tilde{\Gamma}^{[\epsilon]}_{n_2}(\tilde{D}),\quad \tilde{D}\geq 1 \tag{78}$$

for fixed electronic energy. The difference by three units between the exponents of the first terms of Eqs. (77) and (78) arises from the factor $\tilde{\delta}_n^{3/2}$ in Eq. (57). By using Eqs. (29) and (35), we transform the scaling laws (77) and (78) back to the representation in terms of the original ion-surface distance D:

$$\Gamma^{[Z]}_{n_1}(D)=\left[\frac{n_2}{n_1}\right]^{9/2}[\Xi(D/D_{n_1})]^{n_1-n_2}\Gamma^{[Z]}_{n_2}(n_2^2D/n_1^2) ,\quad D\geq D_{n_1} \tag{79}$$

and

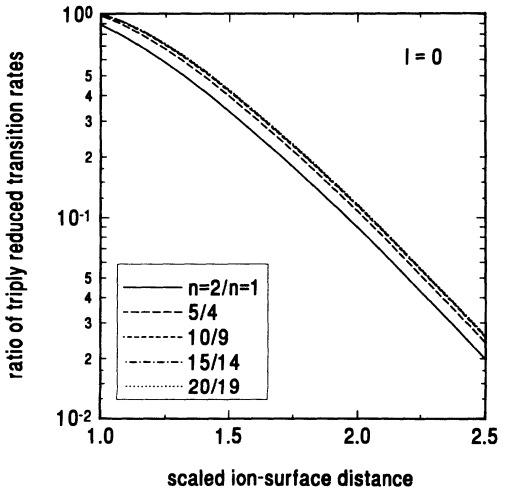

FIG. 13. Ratios of doubly reduced transition rates γ_n for a sequence of pairs of adjacent n values, plotted as a function of the scaled ion-surface distance $\tilde{D}$.

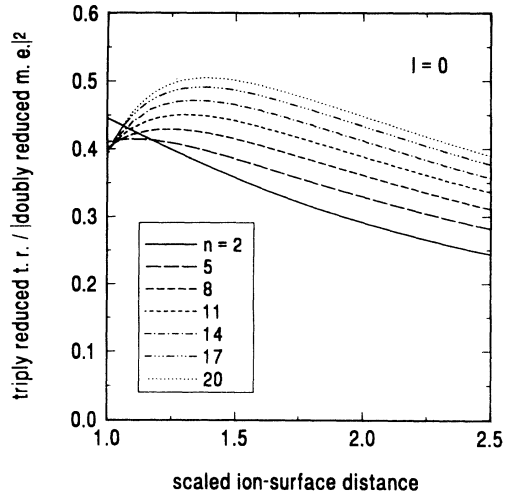

FIG. 14. Ratios of triply reduced transition rate $\bar{\gamma}_n$ to square modulus of (normalized) doubly reduced transition matrix element $\bar{M}_n$ at $\tilde{k}_\parallel=0$ for a sequence of n values, plotted as a function of the scaled ion-surface distance $\tilde{D}$. For normalization of the matrix elements, see text.

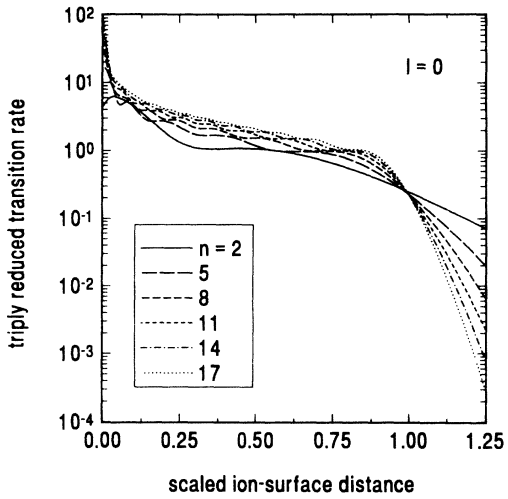

FIG. 15. Triply reduced transition rates $\bar{\gamma}_n$ for a sequence of n values, plotted as a function of the scaled ion-surface distance $\tilde{D}$.

$$\Gamma_{n_1}^{[\epsilon]}(D)=\left[\frac{n_2}{n_1}\right]^{3/2}[\Xi(D/D_{n_1})]^{n_1-n_2}\Gamma_{n_2}^{[\epsilon]}(n_2D/n_1)\ , \qquad D\geq D_{n_1}\ . \tag{80}$$

When used in the approximate calculation of transition rates from known rates, the scaling laws (75)–(80) are, because of the faster convergence in Eq. (74), evidently much more accurate than are the corresponding laws (63)–(67) in the calculation of $\tilde{k}_\parallel=0$ transition matrix elements at the same n_1 and n_2.

Combining Eqs. (61) and (74), we conclude that the ratio $\bar{\gamma}_n(\tilde{D})/|\bar{M}_n(0;\tilde{D})|^2$ converges towards an (n-independent) *universal* function $\Upsilon(\tilde{D})$. In order to improve the convergence, we define $\Upsilon(\tilde{D})$ with respect to "normalized," doubly reduced matrix elements, which are required to attain at $\tilde{D}=1$ the value $\bar{M}_\infty(0;1)$ (cf. Fig. 8), and write explicitly

$$\bar{\gamma}_n(\tilde{D})=\Upsilon(\tilde{D})|\bar{M}_n(0;\tilde{D})|^2\frac{|\bar{M}_\infty(0;1)|^2}{|\bar{M}_n(0;1)|^2},\quad \tilde{D}\geq 1 \tag{81}$$

as an approximation relation for finite n. In Fig. 14, we display ratios of triply reduced transition rates to normalized, doubly reduced $\tilde{k}_\parallel=0$ matrix elements for a sequence of n values. The convergence is seen to be still slow, but the curve corresponding to $n=20$ is expected to provide a fairly good numerical approximation to $\Upsilon(\tilde{D})$.

2. *The classically allowed range*

In the range $\tilde{D}<1$, the qualitative behavior of the triply reduced transition rates $\bar{\gamma}_n$ appears to be different from that of the doubly reduced matrix elements $\bar{M}_n$. While the oscillations of the latter quantities tend to persist with roughly constant amplitude when n becomes large (cf. Fig. 7), the rates shown in Fig. 15 exhibit, for $\tilde{D}>0$, a tendency for convergence towards a smooth limiting curve. We are thus tempted to write

$$\lim_{n\to\infty}\bar{\gamma}_n(\tilde{D})=\Omega(\tilde{D}),\quad 0<\tilde{D}<1\ , \tag{82}$$

with a *universal* function $\Omega(\tilde{D})$. Since, according to Eqs. (57) and (72), $\bar{\gamma}_n(0)$ diverges in the limit $n\to\infty$, the convergence in Eq. (82) is supposed to be nonuniform. This is an irrelevant feature as long as Eq. (82) is used as an approximate relation for finite n. A fairly good numerical approximation to $\Omega(\tilde{D})$ is given by the uppermost of the curves of Fig. 15. In the range $0.2<\tilde{D}<0.9$ the latter curve follows an exponential dependence.

It is instructive to transform Eq. (82), for finite n, to the unscaled representation for the full transition rate $\Gamma_n^{(Z;V_0)}(D)$. Using Eq. (35), (52), and (57), and (72), we find

$$\Gamma_n^{(Z;V_0)}(D)=\frac{2^{3/2}}{\pi}\frac{Z^3}{V_0^{1/2}n^{9/2}}\Omega(ZD/2n^2)\ , \qquad 0<D<2n^2/Z\ . \tag{83}$$

In conjunction with the numerical approximation to the function $\Omega(D)$ provided by Fig. 15, Eq. (83) gives a very simple, explicit representation of the transition rate in the classically allowed range.

The convergence of the rates $\bar{\gamma}_n(\tilde{D})$ towards the limiting function $\Omega(\tilde{D})$ is fairly slow (cf. Fig. 15). So, from the point of view of applications, it is useful to adopt also the procedure leading to Eqs. (69) and (70) for the $\tilde{k}_\parallel=0$ matrix elements in order to extend the scaling laws for the transition rates into the classically allowed range. By eliminating the function $\Xi(\tilde{D})$ from Eq. (74), we find for arbitrary $\tilde{D}$

$$\bar{\gamma}_{n_1}(\tilde{D})=\left[\frac{\bar{\gamma}_{n_3}(\tilde{D})}{\bar{\gamma}_{n_4}(\tilde{D})}\right]^{n_{12}/n_{34}}\bar{\gamma}_{n_2}(\tilde{D}) \tag{84}$$

and

$$\bar{\gamma}_{n_1}(\tilde{D})=\frac{[\bar{\gamma}_{n_2}(\tilde{D})]^{n_{13}/n_{23}}}{[\bar{\gamma}_{n_3}(\tilde{D})]^{n_{12}/n_{23}}} . \quad (85)$$

An example demonstrating the suitability of Eq. (85) is given in Ref. 36.

VI. DISCUSSION

We now present a summarizing discussion of our results and make some brief remarks concerning quasiclassical aspects and possible applications of these results as well as possible extensions of our analysis.

A. Summary of results

The general result of the theoretical analysis performed in this paper is that, within the framework set by our model assumptions, resonant electron transfer in ion–metal-surface interactions exhibits pronounced universal behavior and obeys simple scaling laws. A clue to this finding lies apparently in our selection of the classical threshold distance as a scaling parameter for the ion-surface distance.

From the formal analysis of Sec. IV, the factorized form (47) of the reduced transition matrix element $\tilde{M}^{(Z)}_{nlm}(\tilde{k}_{\parallel};\tilde{D})$ has emerged as a central result. This allows the full matrix element $\tilde{\mathcal{M}}^{(Z;V_0)}_{nlm}(\tilde{k}_{\parallel};\tilde{D})$ to be expressed essentially in terms of the doubly reduced matrix $\bar{M}_{nlm}(\tilde{k}_{\parallel};\tilde{D})$, which is independent of the parameters Z and V_0 that characterize the strength of the electronic potentials in the initial and final states. The universal behavior expressed by this independence reflects scaling properties of the perturbing potential and of the wave functions we use to describe the initial and final electronic states. Notably, Eq. (47) holds exactly for arbitrary ionic quantum numbers n,l,m, although the scaling parameters depend on n only. The specific symmetry properties of hydrogenic wave functions are likely to be responsible for this feature.

As a consequence of Eq. (47), the transition rate $\tilde{\Gamma}^{(Z;V_0)}_{nlm}(\tilde{D})$ can be expressed in terms of the reduced rate $\bar{\Gamma}^{(\tilde{\delta}_n)}_{nlm}(\tilde{D})$. This rate depends on Z and V_0 via the scaled orbital binding energy $\tilde{\delta}_n$ only. In the large-n limit, the reduced rate can in turn be expressed in terms of the doubly reduced rate $\gamma_{nlm}(\tilde{D})$, which is independent of the potential parameters.

Using the results of Sec. IV as well as detailed evidence obtained from explicit calculations, we have systematically analyzed in Sec. V the large-n limit of transition matrix elements and rates for the specific case $l=0$. The principal result is that the behavior of the matrix elements and rates is, to a large extent, governed by three universal functions which depend on the scaled ion-surface distance $\tilde{D}$ only.

The function $\Xi(\tilde{D})$ determines ratios of squared $\tilde{k}_{\parallel}=0$ matrix elements for different n values in the classically forbidden range, as expressed by the scaling law (63) and its specific forms. From Eq. (63), the more general scaling laws (69) and (70) have been inferred. These laws cover the full range of ion-surface distances. It is precisely the function $\Xi(\tilde{D})$ that also enters the scaling law (75) for the triply reduced transition rate $\bar{\gamma}_n(\tilde{D})$. By analogy to Eqs. (69) and (70) for the matrix elements, the more general scaling laws (84) and (85) hold for the transition rates.

The simultaneous appearance of the function $\Xi(\tilde{D})$ in the scaling laws (63) and (75) implies the relation (81) to hold between the transition rates $\bar{\gamma}_n(\tilde{D})$ and the squared matrix elements $|\bar{M}_n(0;\tilde{D})|^2$. This relation involves the universal function $\Upsilon(\tilde{D})$. In Eq. (82), another universal function, $\Omega(\tilde{D})$, emerges as the large-n limit of the triply reduced transition rates $\bar{\gamma}_n(\tilde{D})$ in the classically allowed range. The occurrence of this function has enabled us to write the full transition rate in the simple, explicit form (83).

For the functions $\Xi(\tilde{D})$, $\Upsilon(\tilde{D})$, and $\Omega(\tilde{D})$, we have obtained numerical representations in graphical form. The accuracy of these representations can be improved by performing calculations at n values larger than those considered here. Closed-form representations for the universal functions, it they exist at all, will be extremely difficult to achieve.

While most of the details of the results appear to be at least plausible, some of them remain as a surprise. Examples are the $n^{-3/2}$ law for the doubly reduced transition rate at $\tilde{D}=1$ [cf. Eqs. (72) and (73)] and the occurrence of one and the same universal function in the scaling laws (63) and (75).

B. Quasiclassical aspects

The large-n limit is the quasiclassical limit for the electronic motion in the unperturbed ion. Therefore, the results we have obtained by analyzing transition matrix elements and rates in the large-n limit are supposed to reflect, to some extent, quasiclassical features of resonant electron transfer. To put this conclusion into proper perspective, a few remarks are in order.

Within the adiabatic approximation, one may attempt to analyze the quasiclassical limit by using WKB-type methods directly when solving the stationary Schrödinger equation at fixed ion-surface distance. It turns out, however, that these methods are actually applicable only in the range of asymptotically large distances $D \gg D_n$ (Refs. 27,28), i.e., in the extreme tunneling regime of resonant electron transfer. As the range of physically important ion-surface distances extends from the asymptotic regime far down into the classically allowed range,[7,14] the direct application of WKB methods appears to be not well suited for elucidating quasiclassical features.

When applying the first-order adiabatic approximation, one may think of replacing the unperturbed ionic radial wave function with its WKB approximant.[38] This procedure, however, would destroy for the simple model used here the possibility to evaluate the transition matrix element in closed form. This difficulty is circumvented, at least partly, when large-n approximations are introduced only *after* the reduction of the matrix element to a one-dimensional momentum space integral.[26] Using asymptotic expressions for the radial momentum space wave function,[38] one is then left with an integral whose

properties still have to be explored in detail.

One may, of course, consider resonant electron transfer also from a purely classical point of view. The classical rate for electronic transitions out of the ion into the metal ("electron loss") is given essentially as the product of the frequency associated with the classical Coulomb orbit and the probability for the electron to hit the surface within the area of the potential saddle.[32] This rate is found to be proportional to $1-\tilde{D}$, in contrast to the essentially exponential behavior of the quantal rate at large n in the classically allowed range [cf. Eq. (83) and Fig. 15]. The overall factor Z^2/n^3 in the classical rate differs from the factor $Z^3/n^{9/2}$ in the quantal rate.

C. Applications and extensions

The conceptual framework we have developed here as well as our specific results may find applications in various directions.

Our scaling procedure may be useful as a guideline for introducing scaling concepts into more sophisticated treatments of resonant electron transfer. This pertains, in particular, to the definition of scaling parameters and to the systematic search for reduced quantities depending no longer on the full set of system parameters. The ultimate goal will be a quantitative analysis of the extent to which transition matrix elements and/or transition rates derived from more advanced treatments follow the scaling behavior disclosed within the present model. Prerequisite to such an analysis are systematic calculations within the advanced models, dealing, in particular, with the range of large ionic quantum numbers. Calculations of this kind will clearly be extremely laborious. Nevertheless, it appears that they could be attempted within nonperturbative approaches like the complex-scaling method[29] or the coupled-angular-mode method.[30]

Transition rates determined from our scaling laws or directly from the explicit expression (83) may serve as quantitative input to time-dependent calculations of occupation probabilities of ionic states. Our rates are particularly accurate in the large-n limit, so that the main areas of application are conceived to be in the treatment of resonance neutralization of highly charged ions and of resonance ionization of Rydberg atoms. As the "freezing" distances[6,15] and ionization distances[14] associated with the occupation probabilities appear to be rather insensitive to changes in the transition rates, we believe our results to be applicable also in the small-n range, the more so since their convergence is fairly fast. For applications of this kind as well as for qualitative discussions, it will be helpful to find simple, analytic parametrizations for the $\tilde{D}$-dependent universal functions. A subtle question, to which we do not try to find an answer here, is whether suitably designed experiments might be able to directly reveal scaling behavior of resonant electron transfer. Extensions of the present analysis within the scope of the first-order adiabatic approximation should include the consideration of nonzero ionic angular momenta at all stages of the analysis as well as an adequate treatment of image-potential effects.

While in our general analysis no restriction has been imposed on the values of the quantum numbers l and m, we have confined ourselves to the case $l=0$ when systematically analyzing the limit $n\to\infty$. By invoking continuity arguments, we suppose the results obtained in this limit to hold also for fixed $l>0$. However, if we consider the case of finite n and if we aim at deriving scaling laws for the case of fixed n and varying l and m, we have to take into account the l and m dependence explicitly in the scaling procedure. Without entering a systematic discussion, we suspect that for $m=0$ it will be appropriate to scale the ion-surface distance in terms of the l-dependent classical threshold distance

$$D_{nl}=\frac{n^2}{Z}\{1+[1-l(l+1)/n^2]^{1/2}\}$$
$$\equiv\frac{D_n}{2}\{1+[1-l(l+1)/n^2]^{1/2}\}\ , \tag{86}$$

which is obtained, in generalization of Eq. (29), by taking into account the centrifugal term in the one-electron potential. As this potential, and consequently the classical threshold distance, do not depend on m, i.e., on the orientation of the ionic orbital with respect to the surface normal, one has to look for a more general parameter to introduce an m-dependent scaling of the ion-surface distance. A possible choice for this parameter is the quantity $[\langle z^2\rangle_{nlm}]^{1/2}$, where $\langle z^2\rangle_{nlm}$ is the expectation value of z^2 in the state with wave function $\psi^{(Z)}_{nlm}(\mathbf{r})$. This quantity provides a simple measure for the spatial extent of the ionic orbital along the surface normal.[14]

We note that when using hydrogenic wave functions to describe the ionic states, one may work in the parabolic (Stark) representation instead of the spherical representation (the use of the Stark representation is indicated in cases where orbital hybridization[29] is strong). Formally, these representations are completely equivalent as they are connected by a unitary transformation.[49] We could therefore think of exploiting this transformation to derive scaling laws for resonant electron transfer in the Stark representation from the laws in the spherical representation. This procedure, however, would presuppose that we were able to infer scaling laws connecting the different l substates of a given n manifold. As long as this has not been achieved, we may envisage an independent analysis of scaling properties in the Stark representation. The shape of the wave function associated with a Stark state is characterized by its dipole moment. Therefore, this quantity may serve as a starting point for defining an appropriate scaling parameter for the ion-surface distance.

In order to deal with image-charge effects, we would have to include them not only in the scaling parameters, but also in the perturbing potential. Then, however, the transition matrix elements are no longer amenable to a closed-form evaluation, and so a systematic treatment of these effects is beyond the scope of the present work. Adopting in this situation a heuristic view, we may assume that the general structure of our results is not severely affected by image-charge effects and that quantitative changes are mainly brought about by the change in the classical threshold distance. We may then suggest to use, at least for qualitative considerations, one or the oth-

er of our results with the scaling parameter D_n replaced with the classical threshold distance for the full one-electron potential including the image potentials.

A comment is in order regarding the influence which the choice of the density of conduction-band states has on our results. In specific cases, the realistic density may exhibit an energy dependence departing considerably from that of the free-electron density assumed in the present analysis. The influence of the density of states will be strongest in those of our results in which transition rates at substantially different electronic energies are connected. This is the case for the fixed-Z scaling laws at small n values. On the other hand, in the scaling laws for fixed κ_n, i.e., for fixed electronic energy, the density of states apparently cancels out.

VII. CONCLUDING REMARKS

In conclusion, we wish to emphasize the necessity of studying scaling properties of electronic processes in ion–metal-surface interactions. Resonant electron transfer is only one process among a variety of electron-transfer and emission processes, which are strongly coupled in general and which influence the observable properties of the ion-metal system in an intricate way. For an adequate understanding of the interaction, the contributions from the individual processes must be disentangled by performing detailed analyses. To achieve this goal, one has to work within a theoretical frame that is simple enough to be tractable and yet keeps the essential physical information. In this situation, scaling concepts appear to be well suited for identifying those parameters which primarily determine the characteristics of the various processes, and for simplifying actual calculations.

In the present paper, we have demonstrated the usefulness of scaling concepts for analyzing resonant electron transfer, which is a genuine one-electron process. As a next step, one may envisage the analysis of Auger-type two-electron processes. These processes involve, on the level of the transition matrix elements, a larger number of parameters than the one-electron process and therefore require the introduction of a more general scaling scheme. The greater complexity of the two-electron processes will make simplifications arising from the application of scaling concepts particularly welcome.

APPENDIX A: JELLIUM WAVE FUNCTIONS

For the bound-state case $k_z^2/2 < V_0$, the jellium wave functions corresponding to the potential (4) read[26]

$$\phi_{\mathbf{k}}^{(V_0)}(\mathbf{r}) = \exp(ik_x x)\exp(ik_y y) g_{k_z}^{(V_0)}(z) , \tag{A1}$$

where

$$g_{k_z}^{(V_0)}(z) = [\exp(ik_z z) + a\exp(-ik_z z)]\Theta(-z) + b\exp(-\kappa_z z)\Theta(z) \tag{A2}$$

and

$$\kappa_z = (2V_0 - k_z^2)^{1/2} > 0 . \tag{A3}$$

The reflection coefficient a and the penetration coefficient b are given by

$$a = \frac{k_z - i\kappa_z}{k_z + i\kappa_z}, \quad |a| = 1 \tag{A4}$$

and

$$b = \frac{2k_z}{k_z + i\kappa_z} \equiv 1 + a, \quad |b|^2 = \frac{2k_z^2}{V_0} , \tag{A5}$$

respectively. When normalized over an infinitely large volume, the wave functions (A1) satisfy the condition

$$\langle \phi_{\mathbf{k}}^{(V_0)} | \phi_{\mathbf{k}'}^{(V_0)} \rangle = (2\pi)^3 \delta^3(\mathbf{k} - \mathbf{k}') . \tag{A6}$$

If the resonance condition (10) is fulfilled, we can rewrite $|b|^2$ in the form

$$|b|^2 = \frac{2}{V_0}(k_n^2 - k_\parallel^2) , \tag{A7}$$

where $k_\parallel$ is defined by Eq. (22). The wave function $\phi_{\mathbf{k}}^{(V_0)}(\mathbf{r})$ in the range $z \geq 0$ can be written in the resonant case as

$$\phi_{\mathbf{k}}^{(V_0)}(\mathbf{r}) \equiv \phi_{\mathbf{k}_\parallel}^{(Z;V_0)}(\mathbf{r}) = b\chi_{\mathbf{k}_\parallel}^{(\kappa_n)}(\mathbf{r}) , \tag{A8}$$

where the reduced wave function

$$\chi_{\mathbf{k}_\parallel}^{(\kappa_n)}(\mathbf{r}) = \exp(ik_x x)\exp(ik_y y)\exp[-(k_\parallel^2 + \kappa_n^2)^{1/2} z] \tag{A9}$$

depends on Z via the Z dependence of κ_n, but no longer on V_0 and k_z. As the transition matrix elements depend on the azimuthal angle about the k_z axis via an overall phase factor only, it is sufficient for our purposes to assume that the vector $\mathbf{k}$ lies in the (x,z) plane. The reduced wave function is accordingly written in the form

$$\chi_{k_\parallel}^{(\kappa_n)}(\mathbf{r}) = \exp(ik_\parallel x)\exp[-(k_\parallel^2 + \kappa_n^2)^{1/2} z] . \tag{A10}$$

APPENDIX B: CLOSED-FORM EXPRESSION FOR REDUCED TRANSITION MATRIX ELEMENTS

The closed-form expression derived in Ref. 26 for the transition matrix element $\mathcal{M}_{nlm}^{(Z;V_0)}(\mathbf{k};D)$ is rather involved and will not be repeated in full detail here. For our purposes, it is sufficient to write the doubly reduced matrix element $\overline{M}_{nlm}(\tilde{k}_\parallel;\tilde{D})$ defined by Eq. (48) in the compact form [cf. Eqs. (90) and (70)–(72) of Ref. 26]

$$\overline{M}_{nlm}(\tilde{k}_\parallel;\tilde{D}) = (2\pi)^{3/2}\tilde{k}_\parallel^m (2\tilde{k}_+^2)^{-n} \times \exp(-2n\tilde{k}_+\tilde{D}) \sum_{\tau=0}^{n} G_{nlm}^{(\tau)}(\tilde{k}_\parallel^2)[2n\tilde{k}_+\tilde{D}]^{n-\tau} \tag{B1}$$

$(m \geq 0)$, where

$$\tilde{k}_+ = (\tilde{k}_\parallel^2 + 1)^{1/2} . \tag{B2}$$

The function $G_{nlm}^{(\tau)}(\tilde{k}_\parallel^2)$ is a polynomial of degree

$n-(l+m)/2-1$ in $\tilde{k}_\parallel^2$ if $l+m$ is even, and can be written as $\tilde{k}_+$ times a polynomial of degree $n-(l+m+1)/2-1$ in $\tilde{k}_\parallel^2$ if $l+m$ is odd. For $l=0$, in particular, $\overline{M}_n(\tilde{k}_\parallel;\tilde{D})$ depends on $\tilde{k}_\parallel$ via $\tilde{k}_\parallel^2$ only.

After averaging over the oscillatory structure, the magnitude of the matrix element $\overline{M}_n$ appears to be a monotonically decreasing function of $\tilde{k}_\parallel$. We may characterize the decrease in terms of the width Δ_n ("half width at half maximum") associated with the $\tilde{k}_\parallel$ dependence of the *squared* matrix element $|\overline{M}_n|^2$ at fixed $\tilde{D}$. For not too small $\tilde{D}$, the exponential term in Eq. (B1) is expected to dominate the $\tilde{k}_\parallel$ dependence of the matrix element. We then find

$$\Delta_n=\left[\left[1+\frac{\ln 2}{4n\tilde{D}}\right]^2-1\right]^{1/2}, \tag{B3}$$

and, for large n,

$$\Delta_n\approx\left[\frac{\ln 2}{2n\tilde{D}}\right]^{1/2}\equiv 0.589(n\tilde{D})^{-1/2}. \tag{B4}$$

This estimate breaks completely down at $\tilde{D}=0$. It follows from Eq. (B1) that at this point the falloff behavior of $|\overline{M}_n|^2$ in the range $\tilde{k}_\parallel\gg 1$ is independent of n:

$$|\overline{M}_n(\tilde{k}_\parallel;0)|^2\propto\tilde{k}_\parallel^{-4},\quad \tilde{k}_\parallel\gg 1. \tag{B5}$$

At $\tilde{k}_\parallel=0$ and $\tilde{D}=0$, the $l=0$ matrix elements can be shown to attain a common, n-independent value:

$$|\overline{M}_n(0;0)|^2=\pi. \tag{B6}$$

[1]If not further specified, the term "ion" is understood to comprise *positive* ions as well as neutral atoms.

[2]H. D. Hagstrum, in *Inelastic Ion-Surface Collisions,* edited by N. H. Tolk, J. C. Tully, W. Heiland, and C. W. White (Academic, New York, 1977), p. 1.

[3]H. D. Hagstrum, in *Electron and Ion Spectroscopy of Solids,* edited by L. Fiermans, J. Vennik, and W. Dekeyser (Plenum, New York, 1978), p. 273.

[4]R. Brako and D. M. Newns, Rep. Prog. Phys. **52**, 655 (1989).

[5]A. T. Amos, K. W. Sulston, and S. G. Davison, Adv. Chem. Phys. **76**, 335 (1989).

[6]J. Los and J. J. C. Geerlings, Phys. Rep. **190**, 133 (1990).

[7]J. Burgdörfer, in *Review of Fundamental Processes and Applications of Atoms and Ions,* edited by C. D. Lin (World Scientific, Singapore, 1993), p. 517.

[8]H. J. Andrä, in *Physics of Highly Ionized Atoms,* edited by R. Marrus (Plenum, New York, 1989), p. 377.

[9]H. J. Andrä, A. Simionovici, T. Lamy, A. Brenac, G. Lamboley, A. Pesnelle, S. Andriamonje, A. Fleury, M. Bonnefoy, M. Chassevent, and J. J. Bonnet, in *Proceedings of the Seventeenth International Conference on the Physics of Electronic and Atomic Collisions, Brisbane, 1991,* edited by W. R. MacGillivray, I. E. McCarthy, and M. C. Standage (Hilger, Bristol, 1992), p. 89.

[10]F. Aumayr and HP. Winter, Comments At. Mol. Phys. **29**, 275 (1994).

[11]C. Fabre, M. Gross, J. M. Raimond, and S. Haroche, J. Phys. B **16**, L671 (1983).

[12]C. A. Kocher and C. R. Taylor, Phys. Lett. A **124**, 68 (1987).

[13]D. F. Gray, Z. Zheng, K. A. Smith, and F. B. Dunning, Phys. Rev. A **38**, 1601 (1988).

[14]U. Wille, Surf. Sci. **307-309**, 874 (1994).

[15]H. Winter, Comments At. Mol. Phys. **26**, 287 (1991).

[16]H. Winter, in *Proceedings of the Eighteenth International Conference on the Physics of Electronic and Atomic Collisions, Aarhus, 1993,* edited by T. Andersen, B. Fastrup, F. Folkmann, H. Knudsen, and N. Andersen, AIP Conf. Proc. No. 295 (AIP, New York, 1993), p. 751.

[17]G. Betz, Nucl. Instrum. Methods Phys. Res. Sect. B **27**, 104 (1987).

[18]R. Hippler and S. Reinke, Nucl. Instrum. Methods Phys. Res. Sect. B **68**, 413 (1992).

[19]*Desorption Induced by Electronic Transitions (DIET V),* edited by A. R. Burns, E. B. Stechel, and D. R. Jennison (Springer, Berlin, 1993).

[20]D. Teillet-Billy and J. P. Gauyacq, Surf. Sci. **269/270**, 162 (1992).

[21]P. Nordlander, Phys. Rev. B **46**, 2584 (1992).

[22]H. Brenten, H. Müller, and V. Kempter, Phys. Rev. Lett. **70**, 25 (1993).

[23]J. C. Tully, Phys. Rev. B **16**, 4324 (1977).

[24]J. B. Marston, D. R. Andersson, E. R. Behringer, B. H. Cooper, C. A. DiRubio, G. A. Kimmel, and C. Richardson, Phys. Rev. B **48**, 7809 (1993).

[25]H. Shao, D. C. Langreth, and P. Nordlander, in *Low-Energy Ion-Surface Interactions,* edited by J. W. Rabalais (Wiley, New York, 1994), p. 117.

[26]U. Wille, Phys. Rev. A **45**, 3004 (1992).

[27]A. V. Chaplik, Zh. Eksp. Teor. Fiz. **54**, 332 (1968) [Sov. Phys. JETP **27**, 178 (1968)].

[28]R. K. Janev, J. Phys. B **7**, 1506 (1974); **7**, L359 (1974).

[29]P. Nordlander and J. C. Tully, Phys. Rev. B **42**, 5564 (1990).

[30]D. Teillet-Billy and J. P. Gauyacq, Surf. Sci. **239**, 343 (1990).

[31]A. Borisov, D. Teillet-Billy, and J. P. Gauyacq, Nucl. Instrum. Methods Phys. Res. Sect. B **78**, 49 (1993).

[32]J. Burgdörfer, P. Lerner, and F. W. Meyer, Phys. Rev. A **44**, 5674 (1991).

[33]J. N. Bardsley and B. M. Penetrante, Comments At. Mol. Phys. **27**, 43 (1991).

[34]J. Burgdörfer and F. Meyer, Phys. Rev. A **47**, R20 (1993).

[35]U. Wille, Surf. Sci. Lett. **280**, L291 (1993).

[36]U. Wille, Nucl. Instrum. Methods Phys. Res. Sect. B **90**, 295 (1994).

[37]We disregard kinematic effects due to the motion of the ion parallel to the surface, which can be taken into account within the adiabatic approximation by shifting the Fermi sphere of the metal electrons; see Ref. 15.

[38]H. A. Bethe and E. E. Salpeter, in *Handbuch der Physik,* edited by S. Flügge (Springer, Berlin, 1957), Vol. 35, p. 88.

[39]A. Zangwill, *Physics at Surfaces* (Cambridge University Press, Cambridge, 1988), Chap. 4.

[40]L. S. Rodberg and R. M. Thaler, *Introduction to the Quantum Theory of Scattering* (Academic, New York, 1967), Chap. 7.2.

[41]J. W. Gadzuk, Surf. Sci. **6**, 133 (1967); **6**, 159 (1967).

[42]Note that the matrix elements of the metal potential V_m are identical, up to a factor, to the corresponding *overlap* matrix

elements, restricted to the range $z<0$.

[43]A. A. Almulhem and M. D. Girardeau, Surf. Sci. **210**, 138 (1989); A. A. Almulhem, Surf. Sci. **304**, 191 (1994).

[44]A normalization factor that arises from the requirement $\langle\hat{\phi}|\hat{\phi}\rangle=\langle\phi|\phi\rangle$ has been disregarded in Eq. (15). This amounts to neglecting corrections of order $|\langle\phi|\psi\rangle|^2/\langle\phi|\phi\rangle$.

[45]When considering a transition matrix element in which the initial state $|\psi\rangle$ is orthogonalized with respect to the final state $|\phi\rangle$, one also encounters a term which cannot be evaluated in closed form.

[46]Whenever we write transition matrix elements and rates without the labels l and m, this is meant to imply the case $l=0$.

[47]U. Wille, Nucl. Instrum. Methods Phys. Res. Sect. B **67**, 132 (1992).

[48]Equivalently, one could introduce the binding energy of the ionic orbital, $|\epsilon_n|$, as a scaling parameter. For a discussion of the large-n limit, however, the choice V_0 is slightly better suited.

[49]D. Park, Z. Phys. **159**, 155 (1960).

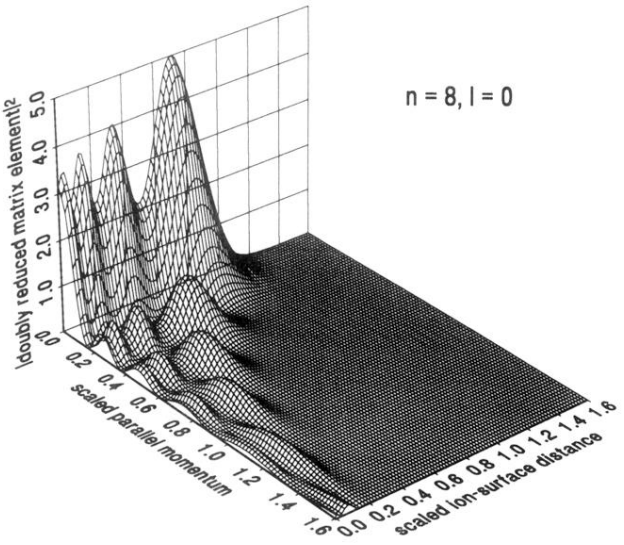

FIG. 3. Square modulus of the doubly reduced transition matrix element $\overline{M}_n$ for $n=8$, plotted as a function of the scaled parallel momentum $\tilde{k}_{\parallel}$ and the scaled ion-surface distance $\tilde{D}$.